Immunity
Article

Regulation of Actin Dynamics by Protein Kinase R Control of Gelsolin Enforces Basal Innate Immune Defense

Aaron T. Irving,[1] Die Wang,[1] Oliver Vasilevski,[1] Olivier Latchoumanin,[1] Noga Kozer,[2] Andrew H.A. Clayton,[2] Anette Szczepny,[1] Hiroyuki Morimoto,[1,3] Dakang Xu,[1] Bryan R.G. Williams,[1] and Anthony J. Sadler[1,*]
[1]Centre for Cancer Research, Monash Institute of Medical Research, Monash University, Clayton, Victoria 3168, Australia
[2]Centre for Microphotonics, Faculty of Engineering and Industrial Sciences, Swinburne University of Technology, Hawthorn, Victoria 3122, Australia
[3]Department of Anatomy, School of Medicine, University of Occupational and Environmental Health, Kitakyushu, Fukuoka, 807-8555, Japan
*Correspondence: anthony.sadler@monash.edu
DOI 10.1016/j.immuni.2012.02.020

SUMMARY

Primary resistance to pathogens is reliant on both basal and inducible immune defenses. To date, research has focused upon inducible innate immune responses. In contrast to resistance via cytokine induction, basal defense mechanisms are less evident. Here we showed that the antiviral protein kinase R (PKR) inhibited the key actin-modifying protein gelsolin to regulate actin dynamics and control cytoskeletal cellular functions under homeostatic conditions. Through this mechanism, PKR controlled fundamental innate immune, actin-dependent processes that included membrane ruffling and particle engulfment. Accordingly, PKR counteracted viral entry into the cell. These findings identify a layer of host resistance, showing that the regulation of actin-modifying proteins during the innate immune response bolsters first-line defense against intracellular pathogens and has a sustained effect on virus production. Moreover, these data provide proof of principle for a concept in which the cell cytoskeleton could be targeted to elicit broad antiviral protection.

INTRODUCTION

In order to mount a sustainable infection, a pathogen must overcome the host's defense mechanisms. This initial resistance to infection is regulated by the innate immune system, which consists of nonspecific basal and inducible resistance components. Through innate immunity the host first resists infection, then upon breach of the defenses of the cell, rapidly responds to induce resistance factors that restrain the pathogen and elicit specific humoral and cell-mediated responses. Our understanding of the inducible innate immune response has been greatly advanced by elucidation of cell signaling pathways mediated by the cytoplasmic helicases retinoic acid-inducible gene I (RIG-I) and MDA5 and by the Toll-like and NOD-like receptors. Activation of these pathogen-recognition receptors potently induces cytokines and inherent inflammatory processes to activate immune cells, thereby curbing infection. There has not, however, been an equivalent advance in our understanding of basal innate immune-resistance processes, because these cellular resistance factors are not distinguished during an infection by conspicuous induction. Hence, the specific factors that instigate this resistance are largely unknown and there is a lack of detail of the molecular mechanisms that enforce basal resistance to pathogens.

A major component of this basal resistance is structural defense, established by mechanical features of the cell. The central component of this is the actin cytoskeleton of the cell. Not only is the cytoskeleton critical for reorganization of the cell membrane during pathogen entry to the cell, but it also organizes host defenses. The actin cytoskeleton arranges pathogen-recognition receptors and recruits cell-signaling intermediates, underpins cellular migration and vesicle movements, and mediates membrane movements in processes such as endocytosis by membrane ruffling and phagocytosis. More than 100 actin-binding proteins have been identified that regulate nucleation and polymerization of monomeric actin to form fibers and higher-order actin structures, or alternatively, sever actin fibers to remodel the cytoskeleton (dos Remedios et al., 2003). Processes that regulate the activity of actin-binding proteins, with resulting consequence to the cytoskeleton, are poorly characterized. Hence, a greater insight into actin dynamics during host-pathogen interaction is needed. Here we identify that the innate immune protein kinase R (PKR) has a previously unrecognized role as an actin modifier through control of the actin-binding protein gelsolin (GSN).

GSN is a constitutively expressed protein that resides in a closed conformation until activation, whereupon the protein binds to and severs large actin filaments, altering cell shape and accelerating retraction of filopodia during motility (Lu et al., 1997; Safiejko-Mroczka and Bell, 2001). GSN also has the ability to cap the barbed ends of filaments and trigger actin nucleation, allowing the formation of lamellipodia and phagocytic cups (Arora et al., 2005; Groves et al., 2008; Mazur et al., 2010). In addition, GSN has been implicated in the crosstalk of signaling events from the membrane to the cytoskeleton, triggered by phospholipid binding (Lin et al., 1997; Sun et al., 1997). Through these functions, GSN controls cell morphology, migration, invasion, and movement of the cell membrane. Aberrant expression of GSN has been correlated with a variety of pathologies (Aidinis

et al., 2005; Asch et al., 1996; Maury et al., 1990). Ablation of GSN in mice generates a number of nonlethal physiological and developmental defects (Chellaiah et al., 2000; Crowley et al., 2000; Furukawa et al., 1997; Witke et al., 1995). Interestingly, the GSN-deleted mouse has altered inflammatory processes, most conspicuously via altered platelet and neutrophil function (Witke et al., 1995). The activity of GSN has previously been shown to be regulated by calcium influx or modifications triggered by protein or lipid interactions with molecules such as phosphatidylinositol-4,5-biphosphate (PtdIns(4,5)P_2). A role for GSN in the innate immune response has not been investigated. Intriguingly, another member of the GSN family of actin-binding proteins, Flightless 1 (FLI1), has been involved in the innate immune responses via Toll-like receptor (TLR) signaling. FLI1 contains a leucine-rich repeat domain, in addition to the six GSN-like domains, which allows this protein to bind to the TLR adaptor molecule MyD88 (Wang et al., 2006). This function of FLI1 manifests a link between innate immune cell signaling and GSN-like proteins that remodel the actin cytoskeleton.

PKR is an effector molecule of the innate immune system that responds to cellular stress, typically that associated with viral infection. The protein has been established to function in two principal manners: as an inhibitor of protein translation, via control of the eukaryotic initiation factor 2α, and as a cell signaling molecule, by less-well-determined processes. Although not previously linked to cellular morphology, we showed that cells from the PKR-deleted mouse have an altered actin cytoskeleton. Moreover, PKR-deficient cells were altered in actin-dependent processes such as morphology and structural dynamics compared to wild-type (WT) cells. Fittingly, we demonstrated that PKR directly inhibited GSN. Opposing the previously demonstrated dependence for activation by viral RNA, the effect of PKR upon GSN occurred at homeostatic condition, was reinforced by interferon (IFN), which further induced the constitutively expressed PKR, and was lost upon activation of the kinase. Hence, PKR alters the cell cytoskeleton to instigate basal resistance. Consistent with this, PKR was shown to suppress virus entry to the cell. This observed regulation of actin dynamics by an innate immune protein provides insight into molecular mechanisms of cellular resistance to intracellular pathogens.

RESULTS

Innate Immune Regulation of the Cytoskeleton

In the course of culturing murine embryonic fibroblasts (MEFs) ablated for the innate immune protein PKR (encoded by *Eif2ak2*), we observed differences in features of the cell morphology and motility of WT compared to PKR-deficient cells (see below). We attributed this to fundamental changes in the cell cytoskeleton, because *Eif2ak2*$^{-/-}$ cells were found to have altered actin filaments (Figure 1A). Primary WT and PKR-deficient MEFs were examined for differences in actin stress fiber formation after growth in reduced serum. Actin fibers were visualized with Alexa 488-labeled phalloidin and quantitated with the Imaris software. Figure 1A shows that cells ablated for PKR were devoid of most large actin protofilaments, had a decrease in the total number of filaments, and had shorter average filament length and a decreased total amount of filamentous actin when compared to WT MEFs. Given the context of the role of PKR in immunity, we considered this observation likely to be of significance in infection.

The actin cytoskeleton is essential to many fundamental cell processes, including immune processes such as membrane ruffling. Membrane ruffling is an important endocytic process in fibroblasts that enables the cell to sample the extracellular environment. We compared the ability of WT or PKR-deficient MEFs to form bilateral membrane ruffles in response to serum, as sections of curved membrane folding onto itself, as described previously (Hedberg et al., 1993; Nobile et al., 2010; Sun et al., 1995). PKR-deficient MEFs display increased membrane ruffling in response to serum treatment (Figure 1B). Because membrane ruffling is inherently linked to particle engulfment, we investigated whether PKR altered endocytic uptake. To this end, cells were incubated with FITC-conjugated dextran molecules and then imaged. As Figure 1C shows, PKR-deficient fibroblasts exhibit increased endocytic uptake of fluorescein isothiocyanate (FITC)-dextran particles, consistent with their increased membrane ruffling. Because no mechanism has been recognized that would account for this, we sought to determine the relevant regulatory processes.

PKR Interacts with the Actin-Binding Protein GSN

To identify proteins that interact with PKR, we performed an immunoprecipitation of PKR from MEFs and identified coimmunoprecipitated proteins by mass spectrometry. The actin-binding protein GSN was identified through this procedure (Figure S1A available online). The association between PKR and GSN was further characterized by Förster's resonance energy transfer (FRET) analysis of fluorescent-tagged protein constructs. GSN was expressed as a cyan fluorescent protein (CFP) fusion, whereas PKR was fused to the full-length Venus fluorescent protein and expressed in HEK293T cells. The observed FRET efficiency demonstrates that a high proportion of the two proteins associate in the cell (Figure 2A). As a comparison, FRET efficiencies were calculated between GSN-CFP and actin. This demonstrates that the proportion of GSN associated with PKR approaches the amount of GSN bound to actin filaments in the cell. The FRET pairing discerned that the association between GSN and PKR was uneven throughout the cell, being highest at regions close to the edge of a cell, though not in the leading edge, an area where functional GSN is known to concentrate during migration (Figures 2A and S1B).

To further probe this interaction, we utilized a bimolecule fluorescence approach. In this method, each protein partner is expressed as a fusion construct with separate halves of the Venus fluorophore (as shown in Figure S2). Proteins that interact allow the two halves of the fluorophore to associate, thereby producing a fluorescent signal. Toward this, GSN and WT, or a series of truncated, PKR constructs were fused to either half of Venus then transfected into HEK293T cells. This demonstrated that GSN interacts with the kinase domain of PKR within the region termed the N-lobe (Figures 2B and S1C). The N-lobe has previously been demonstrated to form the interaction interface between each monomer in the active dimeric enzyme (Dey et al., 2005). Consequently, we measured the interaction between GSN and dimeric PKR by measuring FRET between GSN-CFP and PKR monomers fused separately with each half of the split Venus. Because no FRET was

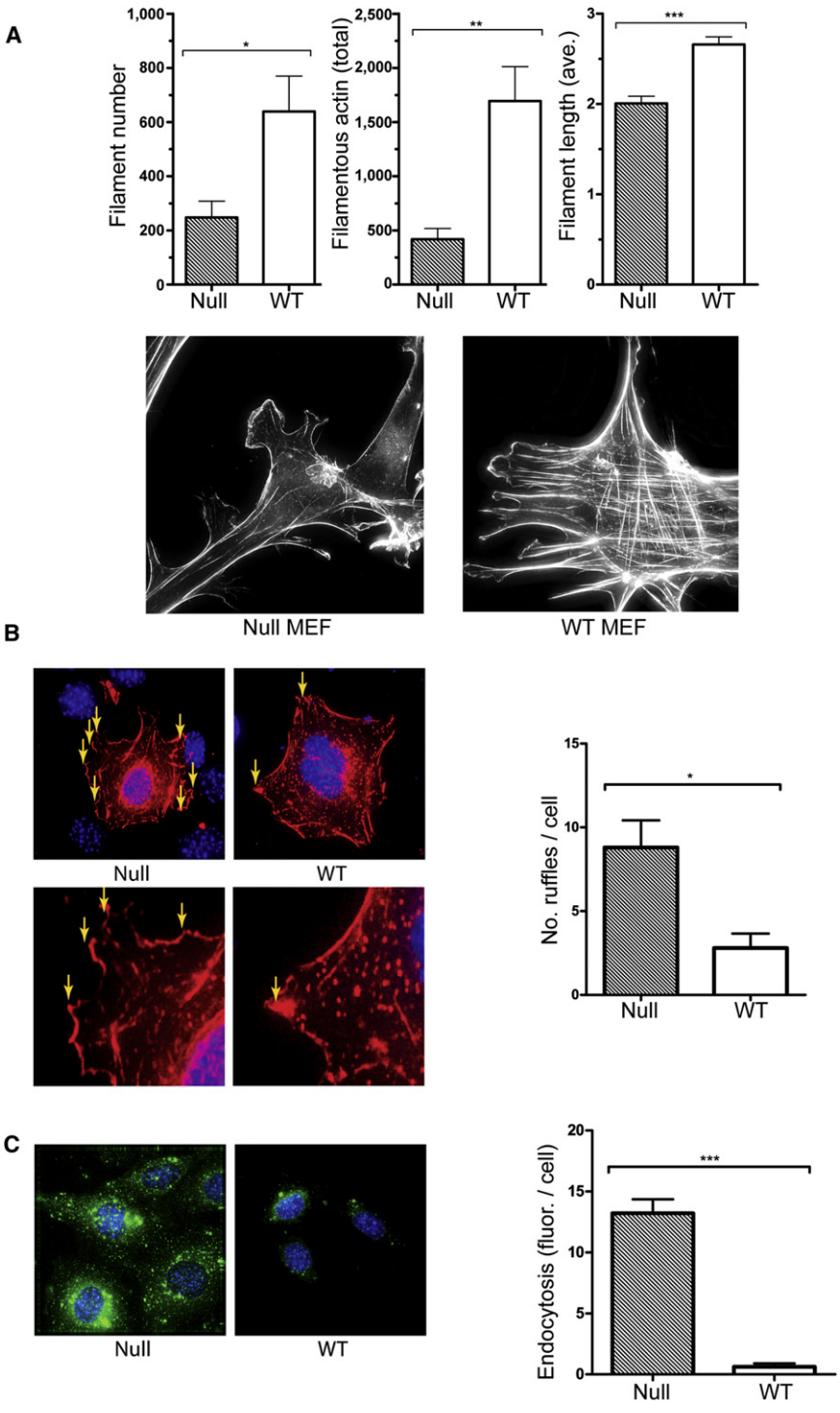

Figure 1. MEFs Ablated for PKR Exhibit Altered Morphology

(A) A quantitation of the state of actin in primary WT and PKR-deficient (null) MEFs. Graphs represent the accumulated data of 50 images for total number of actin filaments, total amount of filamentous actin, and average filament length as quantified by volume rendering in the Imaris software. Example images of primary MEFs are displayed below the graphs as a flattened maximum intensity projection from z stacks for the entire cell. (B) Images of WT and PKR-deficient (null) primary MEFs transfected with mRFP-actin. Cells were fixed, labeled, and imaged for the presence of membrane ruffles (indicated by arrows). Ruffles were visualized in 3D in Imaris as curves of membrane rising off the surface. The lower panel contains magnified projected 2D images for identification of what is considered a "ruffle" and is quantified in the graph on right. Further visualization of ruffles can be seen in Movies S1 and S2. (C) WT and PKR-deficient (null) primary MEFs treated with a 3 kDa FITC-dextran molecule. The amount of dextran internalized (mean fluorescence), through reference to a CellMask plasma membrane stain (removed for image clarity) was quantified with Image J (graphed on the right). Error is displayed as mean ± SEM.

detected in any region of the cell, this strongly suggests that GSN interacts with monomeric, inactive PKR (Figure S1B). Notably, a mutated kinase-dead PKR, in which dimer formation is altered by a point mutation (K296R), bound GSN (Figure 2C). In light of this, we tested the effects of activation stimuli for PKR on the protein association. HeLa cells were treated with the double-stranded (ds) RNA mimetic, polyinosinic:polycytidylic acid (poly(I:C)). Endogenous PKR was immunoprecipitated and coimmunoprecipitation of endogenous GSN was tested by immunoblot. Consistent with the preceding data, PKR and GSN associate under homeostatic conditions but dissociate upon activation of PKR with poly(I:C) (Figures 2D and S1D). Fluorescence lifetime imaging (FLIM)-FRET was used to visualize this temporal protein association between PKR-Venus and GSN-CFP. Basal FRET efficiency was compared to cells after activation of PKR with poly(I:C) or by infection with the herpes simplex virus type 1 (HSV-1), which has been demonstrated previously to activate PKR (Leib et al., 2000). The lifetime of the GSN interaction with PKR is shown, in Figure 2E, as a heatmap within the cell. FLIM-FRET analysis calculated the efficiency of the interaction averaged across whole cells between PKR and GSN to be 11%. This interaction decreased to 3% or 4% upon treatment with HSV-1 or poly(I:C), respectively (Figures 2F, S1E, and S1F). To ensure that the poly(I:C)-mediated decrease in FRET was a specific result of the kinase activation of PKR, the FLIM-FRET was repeated with the kinase-dead mutant K296R PKR. Consistent with the preceding data, poly(I:C) treatment did not decrease FRET between GSN and K296R PKR. Appropriately, there was no poly(I:C)-induced change in the association of GSN with its substrate (Figure 2G). Together,

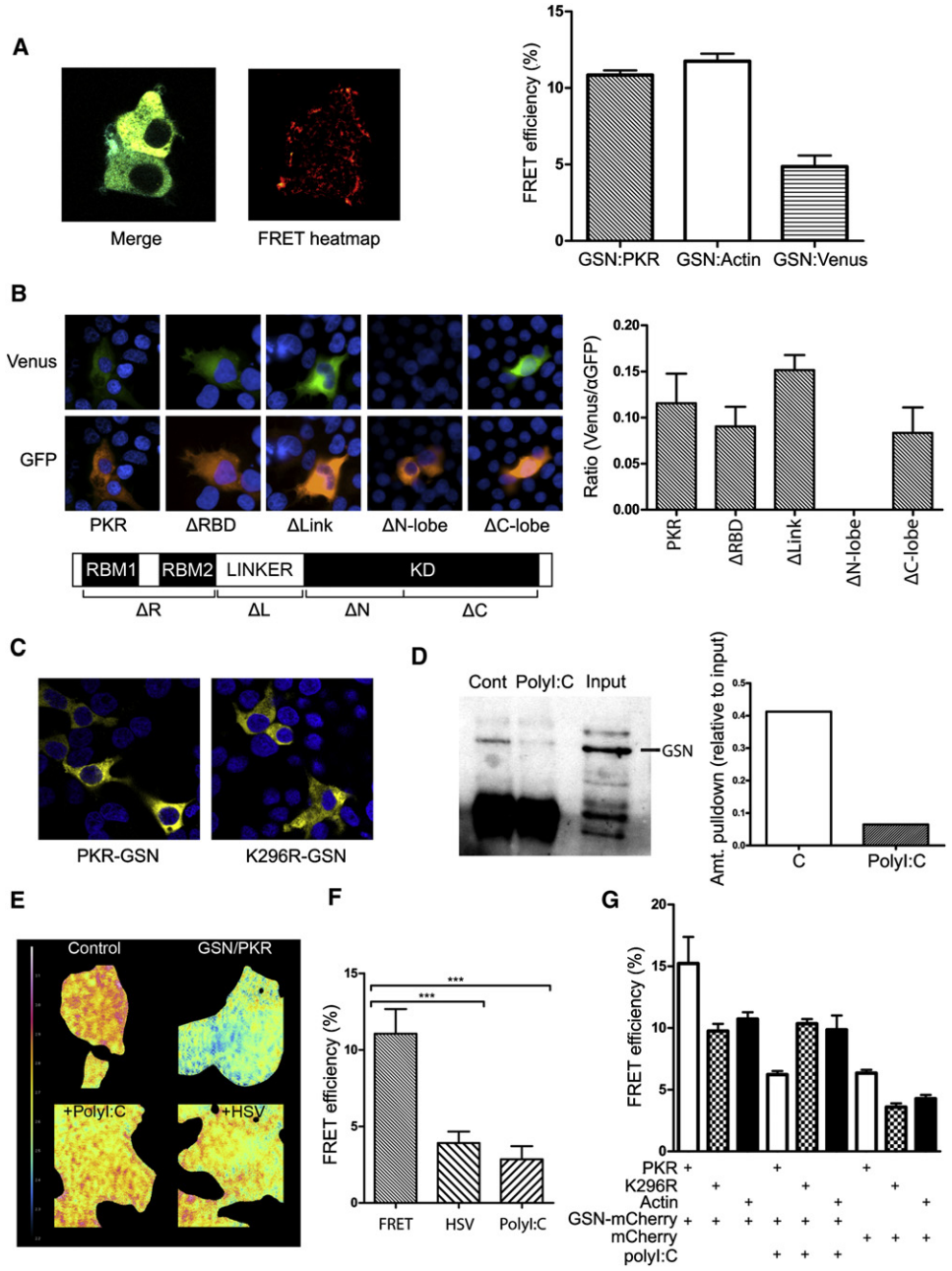

Figure 2. PKR Binds GSN at Homeostatic Conditions

(A) An intensity merged image of CFP-GSN and Venus-PKR transfected HEK293T cells (left) and a heatmap of FRET efficiency, above a 10% cutoff (center), as measured by Acceptor-photobleaching FRET. In the right panel is a graph of FLIM-FRET efficiencies calculated by measuring the shift in donor lifetime with the LI-FLIM software of CFP-GSN after the addition of a FRET acceptor with either PKR or actin-Venus fusions, or Venus alone as a control for nonspecific fluorophore interaction. Additional controls are shown in Figure S1B.

(B) Fluorescence in HEK293T cells formed by interaction of split Venus between GSN fused to V1 and full-length protein (PKR) or constructs lacking the RNA-binding (ΔRBD) and linker (ΔLink) domains, or the N- and C-lobes of the kinase domain (ΔN-lobe and ΔC-lobe, respectively) of PKR fused to V2. Venus fluorescence in cells was normalized to the expression of the various PKR constructs, by detecting the V2 peptide with a GFP antibody (shown on left). A quantitation of approximately 50 images per transfection is graphed on the right.

(C) Fluorescence in HEK293T cells formed by interaction of Venus split between GSN fused to V2 and either WT or kinase-dead PKR (K296) fused to V1. Cell nuclei were detected with Hoechst 3342 stain in (B) and (C).

(D) An immunoblot of proteins immunoprecipitated with a monoclonal antibody to PKR (70/10) from HeLa cell extracts. Cells were untreated (Cont) or treated with poly(I:C) (10 μg/ml) to activate PKR. Proteins were probed with a mouse monoclonal antibody against GSN and quantified (right) relative to the level of GSN in the whole cell lysate (input).

(E) FLIM time-scaled average τp-lifetime images (2.2–3.2 ns) in HEK293T cells with GSN-CFP (control) and GSN-CFP and PKR-Venus untreated (GSN-PKR) and infected with HSV-1, or transfected with poly(I:C). Shorter donor lifetimes indicate the presence of FRET as detected by FLIM.

this analysis shows that GSN and PKR associate at homeostasis but disassociate upon activation of PKR.

Activity of GSN Is Inhibited by the Association with PKR

Because GSN is known to be phosphorylated by other kinases (De Corte et al., 1997), we tested whether GSN was a substrate for PKR in an in vitro kinase assay, as described previously (Sadler et al., 2009). Toward this, glutathione sepharose transferase (GST) GSN constructs were generated, as shown in Figure S2, for kinase assays. However, no phosphorylation of the GSN peptides could be detected (Figures S3A–S3C).

Because our earlier investigations revealed a morphological defect in *Eif2ak2*$^{-/-}$ MEFs, notwithstanding the lack of measurable phosphorylation of GSN, we investigated whether the association with PKR affected the function of GSN. Toward this, an in vitro actin polymerization assay was performed as described elsewhere (Ferjani et al., 2006). In brief, rhodamine-labeled nonnucleated actin monomers were incubated with recombinant functional GSN protein (GSN1-6) or, as a control, a truncated nonfunctional GSN peptide (GSN3-4). In this assay, polymerization of actin monomers induces a fluorescent signal. Figure 3A shows that GSN1-6 reduced the fluorescent signal in accord with its actin-severing ability (see also Figure S3D). Appropriately, the inactive peptide GSN3-4 had no effect. Importantly, the actin-severing activity of GSN1-6 was perturbed by WT recombinant PKR. In keeping with the lack of observed phosphorylation of GSN, the kinase-dead variant of PKR (K296R) similarly inhibited GSN-severing activity (Figure 3A).

To investigate actin dynamics in live cells, fibroblast cell lines were transfected with actin-red fluorescent protein (RFP) and actin filament formation was visualized by fluorescence recovery after photobleaching (FRAP). Fluorescence recovery is dependent upon actin polymerization, which has been established to be strongly dependent on GSN activity (Campbell and Knight, 2007; Halavatyi et al., 2009). Large actin filaments were photobleached and the fluorescence recovery profiles of filaments were measured. Consistent with PKR-dependent inhibition of GSN, MEFs that were ablated for PKR show a markedly reduced rate of fluorescence recovery compared to WT MEFs (Figures 3B and S3E). To confirm that this effect was mediated by PKR, the human PKR genetic locus was reintroduced into PKR-deficient MEFs (coded Bac7) and compared to cells containing the locus but not expressing PKR (Bac10) (Figure S3F). The restoration of PKR expression reinstated the recovery of actin filaments (Figures 3B and S3F; Movies S3 and S4).

GSN-dependent severing of actin alters the ratio of filamentous (F) to monomeric (G) actin. Therefore, the proportion of F- to G-actin was quantitated in WT and PKR-deficient MEFs by labeling with Alexa 488 phalloidin and tetramethyl rhodamine isothiocyanate (TRITC)-deoxyribonuclease-I, respectively. In keeping with the inhibition of GSN activity by PKR shown in vitro, PKR-deficient cell lines had an increased proportion of G-actin compared to WT cells (Figure 3C). This was despite a constant level of GSN expression between cell types (Figure S3G). As performed previously, restoration of PKR expression in MEFs ablated for murine PKR (Bac7) restored the amounts of F-actin compared to the isogenic cells in which the introduced construct was not expressed (Bac10) (Figure 3C). To confirm that the effect of PKR on the actin cytoskeleton was dependent upon GSN, amounts of GSN were reduced in fibroblasts by RNA interference. WT and PKR-deficient fibroblasts were treated with control (lamin A/C) or small interfering RNAs (siRNAs) targeting GSN and actin filaments were visualized as described previously. Figure 3D shows that reduction of GSN rescues the formation of actin filaments in the PKR-deficient cells.

The combined data indicate that the presence of PKR alters the dynamics of actin within a cell by inhibiting GSN-mediated severing of actin filaments. This activity of PKR is apparently independent of its kinase activity.

GSN Is Inhibited by Steric Hindrance

To explain these findings, we propose that the effect of PKR upon actin dynamics is mediated via steric inhibition of the activity of GSN. At homeostasis, GSN forms a spatial arrangement in which the actin-binding domains are inaccessible. Activation of GSN instigates a conformational change to expose its actin-binding domain. We propose that PKR binding prevents this conformational change or otherwise obscures the critical actin-binding domains of GSN. To test this, we measured the proportion of GSN that was bound to actin in the presence or absence of PKR by FLIM-FRET. Figure 4A shows that titration of PKR into *Eif2ak2*$^{-/-}$ cells led to a progressive decrease in the proportion of GSN that associates with actin, confirming that binding of PKR prevents the association of GSN with its substrate.

This was further explored by mutation of GSN. Structural studies show that an α helix encoded by the C-terminal residues of GSN contacts an α helix within the second domain of the molecule, thereby establishing a structural constraint on GSN activity (Burtnick et al., 1997). Deletion of 19 C-terminal residues of GSN (coded GSNCT), including an aspartic acid trimer that has been proposed to mediate the inhibitory intradomain interaction, reduced the association with PKR (Figure 4B). Hence, these data suggest that PKR preferentially associates with the inactive GSN molecule or directly interacts with the C-terminal 19 amino acids of GSN. However, because PKR retains some association with this mutant GSN as well as a GSN peptide that lacked the C-terminal half of the molecule, residues within GSN N-terminal half are sufficient for the interaction (Figure S3H).

Our findings predict that increased amounts of PKR will increase cellular F-actin. In keeping with this, treatment of MEFs with type I IFN, which induces PKR, increased the number of filaments (Figures 4C and S4). Notably, this effect occurred only in the PKR WT cells, demonstrating a strong dependence on PKR for the IFN-dependent increase in actin filaments. A second prediction from our preceding experiments is that

(F) A quantitation of the FLIM-FRET efficiencies from (E) representing FRET efficiency averaged across the whole cell with the LI-FLIM software.
(G) A quantitation of the FLIM-FRET efficiencies between mCherry alone as a control and mCherry tagged to GSN with WT or kinase-dead (K296R) PKR and actin, each tagged with EGFP. Cells are treated (+) with the PKR activator poly(I:C) to test the dependency of the kinase activity of PKR in the interaction with GSN. Error is displayed as mean ± SEM.

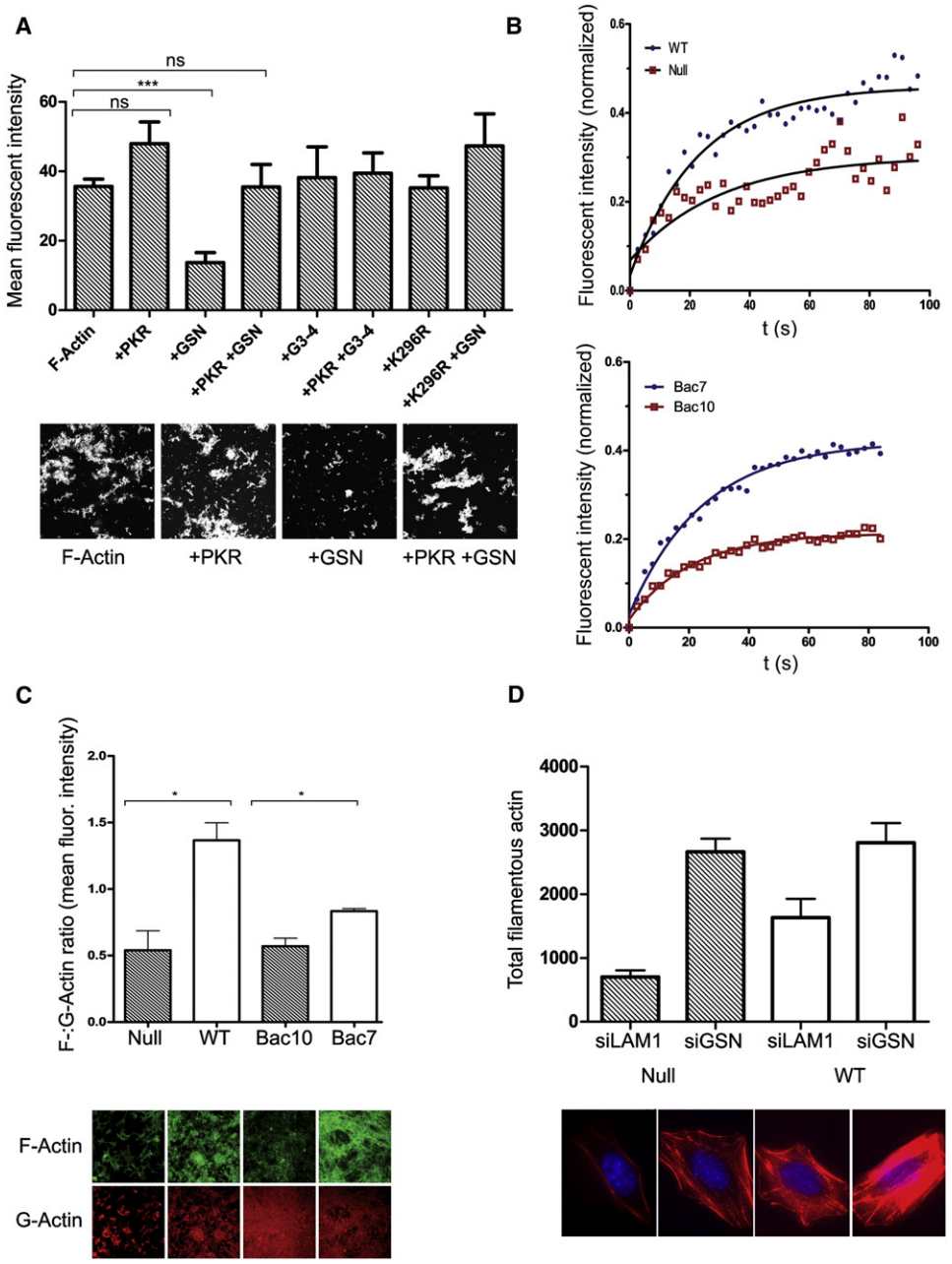

Figure 3. GSN Activity Is Inhibited by PKR

(A) Actin polymerization, measured by fluorescence, was studied in vitro with recombinant rhodamine-labeled actin in the presence or absence of WT (PKR) or kinase-dead PKR (K296R) and GSN peptides encompassing all GSN-like domains, or domains 3–4 of GSN (labeled as GSN and G3-4, respectively). Actin polymerization was quantified as the mean fluorescence intensity for a minimum of 15 fields of view per sample. A representative image of fluorescent actin fragments on glass slides is presented below the graph.

(B) A comparison of actin polymerization rates visualized by FRAP, with mRFP-actin in WT and PKR-deficient MEFs. The graph displays normalized, accumulated data for multiple experiments with a minimum of 35 filaments per cell type, per time point. Points represent mean fluorescence intensity for all filaments; curve indicates one-phase exponential association regressions. This experiment was repeated with PKR-deficient Bac10 cells and the isogenic PKR-reconstituted Bac7 cells.

(C) A quantitation of the ratio of F- to G-actin in various WT and PKR-deficient MEFs. The graph displayed is an accumulation of three independent experiments with an example image for each sample shown below the graph.

(D) A quantitation of the number of Alexa 647-Phalloidin-labeled actin filaments in WT or PKR-deficient MEFs treated with siRNAs against GSN (siGSN) or as a control lamin A/C (siLam1). Representative images shown below the graph are flattened maximum intensity projections of 3D deconvolved z stacks captured on the Deltavision. Constant exposure and contrast settings are used to emphasize differences in filamentous actin staining.

Error is displayed as mean ± SEM.

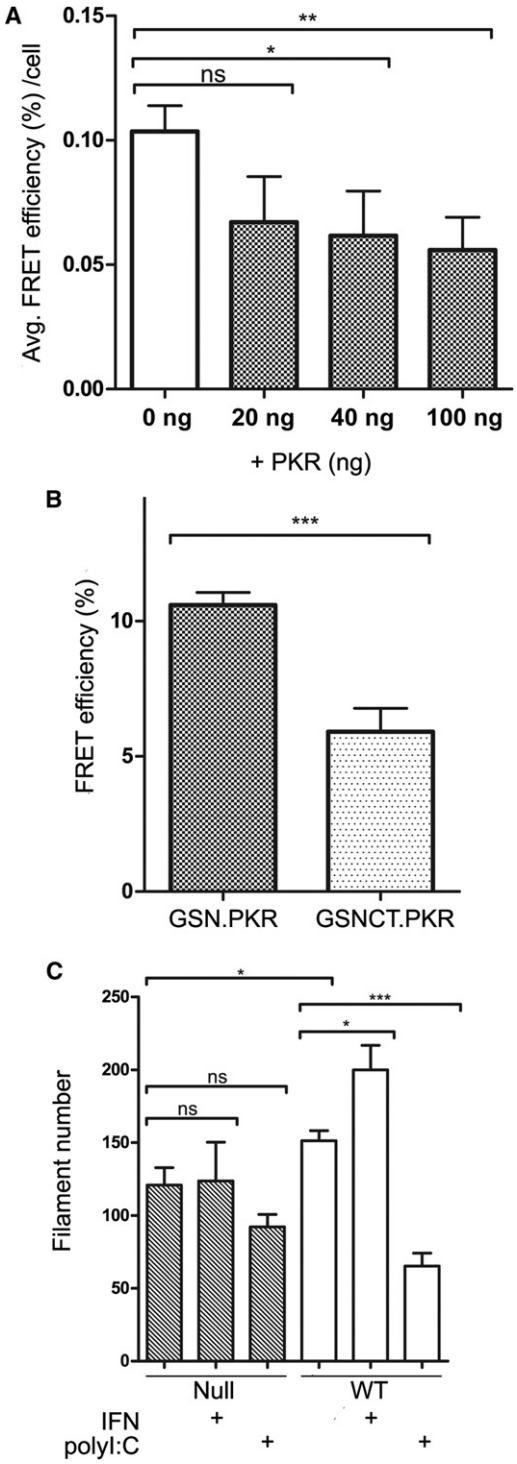

Figure 4. Regulation of GSN by PKR

(A) FLIM-FRET between GSN-CFP and YFP-actin was used to quantitate the association of GSN with actin in PKR-deficient fibroblasts transfected with increasing amounts of a PKR expression construct (at amounts shown).

(B) FLIM-FRET efficiencies observed for the interaction between PKR-Venus and either WT or a 19 amino acid C-terminal truncated mutant (coded GSN and GSNCT, respectively) of GSN-CFP.

(C) Quantified actin filament data, as per Figure 1A, with primary WT or PKR-deficient MEFs treated with murine IFN-α1 (1000 U/ml) and poly(I:C) (10 μg/ml).

activation of PKR should mitigate this PKR-dependent inhibition of GSN. Accordingly, treatment of MEFs with the PKR activator poly(I:C) reduced the actin filaments. Hence, PKR affects actin structure in cells and this effect is dependent upon both the level and activation state of the kinase, as well as the state of GSN.

GSN Controls Virus Uptake, Entry, and Production

Taken together, the initial observed differences in endocytic processes and the preceding results proffer a rationale for the control of GSN by PKR, namely to bolster innate resistance to intracellular pathogens by decreasing uptake by the cell. To test this, we treated fibroblasts with either control or siRNA-targeting GSN, then infected these knockdown cells with human rhinovirus-16 (HRV-16). RNA interference reduced GSN protein amounts by approximately 60% (Figures S5A and S5B). Rhinovirus entry was quantified by probing for the viral VP2 major capsid protein by immunofluorescence. This reduction in GSN was paralleled by a 2-fold reduction in HRV-16 entry into cells (Figure 5A). To ensure that this effect is not limited to the HRV-16, we tested the sensitivity to a second pathogen, HSV-1. WT MEFs were treated with siRNAs as before and then infected with a green fluorescent protein (GFP)-tagged HSV-1 (eGFP-HSV-1). Virus entry to the cell was quantified by demarcating the cell boundary and then measuring GFP fluorescence inside the cell. Figure 5B shows a reduction in the uptake of HSV-1 in the cells treated with an siRNA-targeting GSN. To measure the effect of GSN on virus production and cell survival, the permissive A549 cells were treated with siRNA prior to infection with HRV-16 and HSV-1, cell survival was monitored, and progeny virus was quantified by titrating supernatants 24 hr postinfection onto L929 cells. In keeping with a role for GSN in promoting virus infection, knockdown of GSN reduced HSV-1 production (Figures 5C and S5B–S5D). In addition, HRV-16 produced from GSN knockdown cells exhibited less virus-induced death (Figures 5D, S5D, and S5E).

The observed control of GSN by PKR argues that PKR should similarly inhibit virus entry. To directly test this possibility, we infected WT, PKR-deficient, and MEFs expressing catalytically inactive murine PKR, K271R, equivalent to the K296 of human PKR, with eGFP-HSV-1. PKR-deficient fibroblasts exhibited greater than 2-fold higher virus uptake compared to WT cells. Moreover, the catalytically inactive PKR provided at least comparable protection to the WT protein, consistent with the effects of PKR being independent of direct phosphorylation of GSN and supporting the notion that inactive PKR regulates GSN (Figures 5E and S5F).

To examine the significance of GSN in an in vivo infection, we utilized a murine lung infection model (DuPage et al., 2009). C57BL6/J mice were initially treated by intranasal inhalation of lentivirus expressing either control nontargeting short hairpin (sh)RNA or a pool of four shRNAs targeting GSN to reduce GSN levels in the lung tissue. After 3 days, mice were then similarly infected with a recombinant *LacZ* adenovirus. After a further 4 days, the lungs were harvested and assessed for the levels of GSN and virus-specific β-galactosidase. Immunocytochemistry

One of three experiments is represented with a minimum of 50 cells per sample counted. Error is displayed as mean ± SEM.

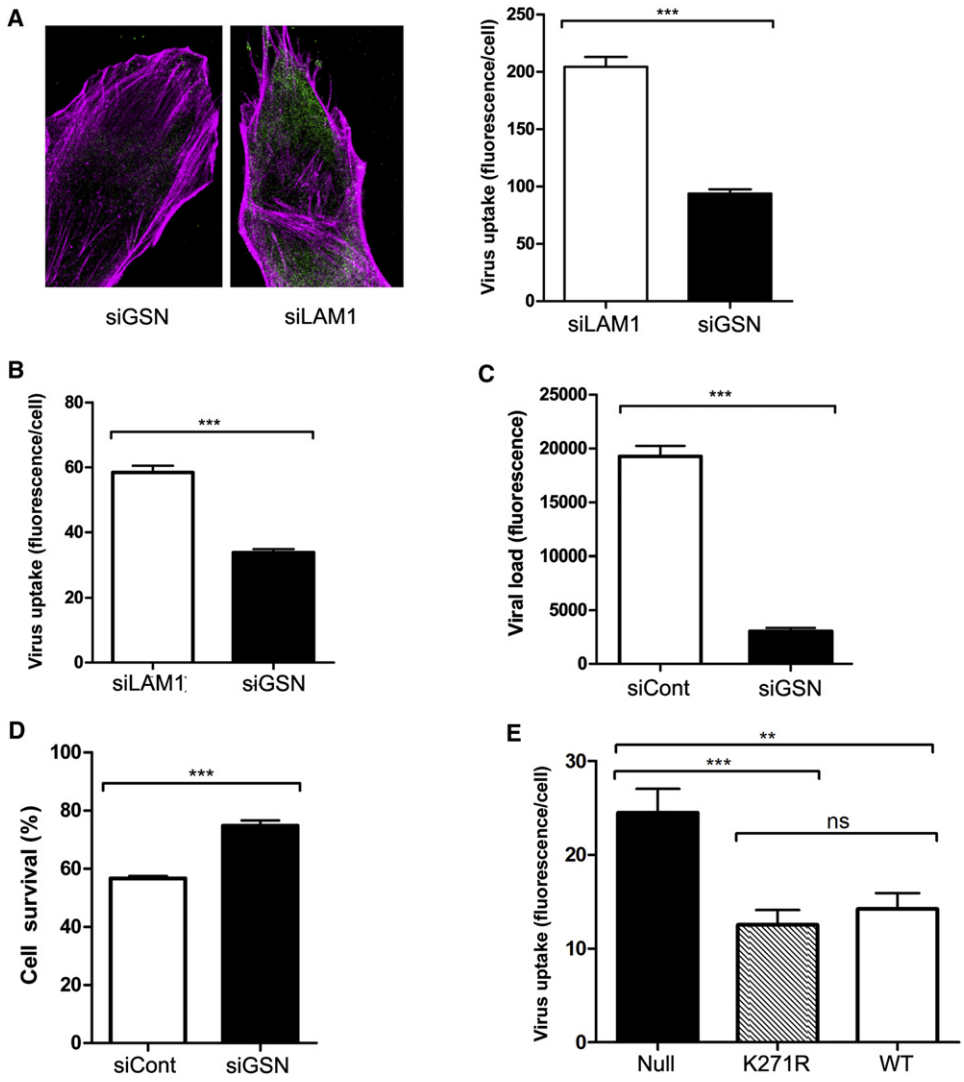

Figure 5. Control of GSN by PKR Affects Virus Entry and Production

(A) Immunofluorescence performed on HRV-16-infected (MOI = 100) MEFs treated with siRNA against GSN (siGSN) or as a control lamin A/C (siLAM1) (left). Levels of HRV-16 within the cell are quantitated 1 hr after infection by immunocytochemical detection of the HRV-16 VP2 capsid protein (green). Actin was labeled with Alexa 647-phalloidin (magenta). The graph (on right) represents the average HRV-16 uptake in three experiments. Images are individual confocal planes from "tile-scanning" (n > 50) with the Zeiss LSM780 confocal.

(B) A quantitation of virus uptake, measured as GFP fluorescence intensity, for MEFs infected with eGFP-HSV-1 (MOI = 100) and treated with siRNAs as per (A).

(C) A quantitation of virus production, assayed by secondary infection of L929 cells, from a primary infection of A549 cells treated with siRNAs as per (A) with eGFP-HSV-1 (MOI = 1). The L929 cells were fixed in formalin and viral load was measured by GFP fluorescence on a GE Typhoon (526 sp filter, 488 nm excitation). The signal was quantified in NIH ImageJ and graphed.

(D) A graph of the survival of *IFNAR1*$^{-/-}$ MEFs 24 hr after infection with HRV-16 produced from a primary infection of A549 cells as per (C). MEFs were rinsed, fixed, and stained with crystal violet and surviving cells were quantitated by measuring absorbance (OD_{595nm}).

(E) A quantitation of virus uptake, measured as GFP fluorescence intensity, for cells expressing WT, catalytically inactive (K271R) PKR, or PKR-deficient (null) MEFs infected with eGFP-HSV-1 as per (B). The phenotype of the cells is shown in Figure S5F.

Imaris was used to demarcate the cell boundary and quantitate the internalized fluorescent signal. The experiment was performed multiple times, in triplicate, with one indicative experiment being displayed. Error is displayed as mean ± SEM.

confirmed reduction of GSN in epithelial cells surrounding alveoli (Figure 6A). Synonymous with this, immunocytochemical staining for the β-galactosidase enzyme directly, or detection of the blue DiX-Indigo precipitate produced by β-galactosidase conversion of X-gal, was markedly decreased with reduced GSN levels (Figures 6B and 6C). These data indicate a significant functional role for the regulation of GSN in restricting virus infection, both in vitro and in vivo.

These results provide a context for the advantage of innate immune regulation of the actin-modifying protein GSN, by which the control of GSN by PKR constitutes a mechanical antiviral mechanism.

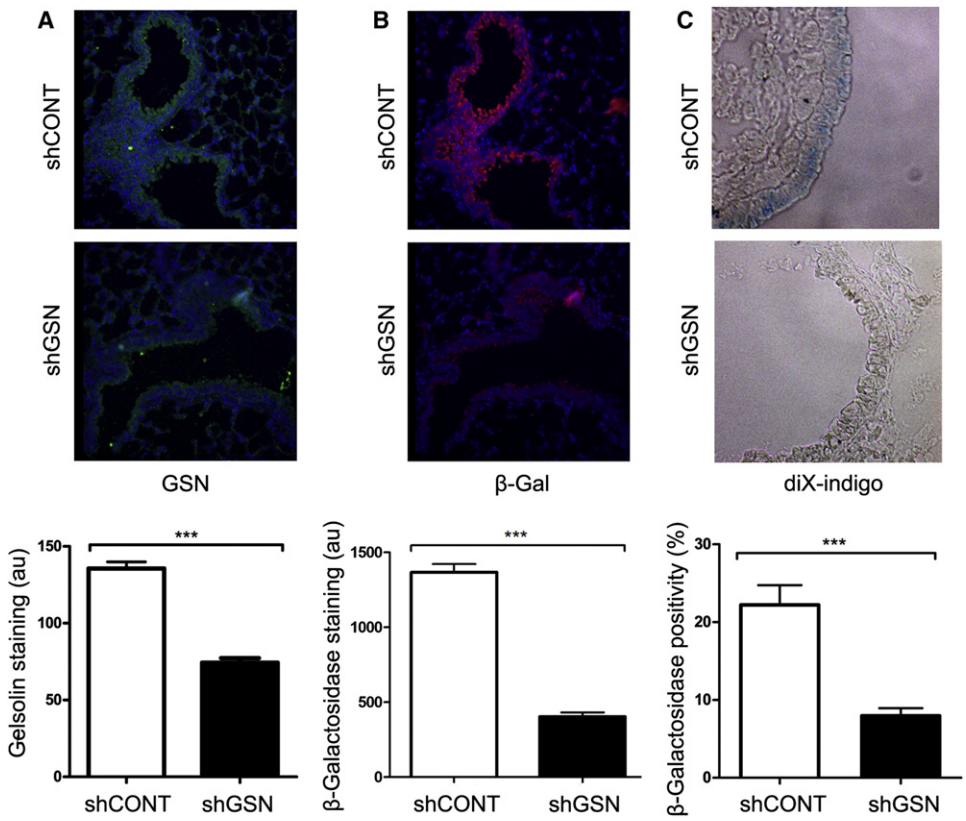

Figure 6. GSN Affects Virus Infection of Murine Lung

(A) GSN levels in cells surrounding the alveoli from mice treated with lentivirus expressing control nontargeting (shCONT) or GSN-targeting (shGSN) shRNAs is graphed at the bottom of the figure, with representative images above. GSN was detected (green) by immunocytochemistry.

(B) A quantitation of the uptake of recombinant adenovirus, as measured by immunocytochemistry of β-galactosidase (β-gal) (red) in alveoli from mice treated with either the control or GSN-targeting shRNAs.

Nuclei are stained with Hoechst 3342 (blue) in (A) and (B).

(C) An alternative quantitation of adenovirus infection in which β-galactosidase activity is measured through the conversion of the colorless X-gal by the enzyme to the blue precipitate (DiX-indigo). The number of blue pixels per image from whole lung sections was calculated with the Metamorph software. The images above the graph are RGB merged trans-illumination light images.

A minimum of 30 images was collected from each of five mice for each group for the analysis. Error is displayed as mean ± SEM.

DISCUSSION

Here we describe an interaction between the actin-binding protein GSN and the protein kinase PKR. This protein interaction is demonstrated to have fundamental biological consequence by regulating the cell cytoskeleton and dependent processes. We show, by both in vitro assay with recombinant proteins and by assessing endogenous function in cells, that PKR inhibits GSN activity. This inhibition occurred with either WT or the kinase-dead PKR mutant (K296R), indicating a kinase-independent function for PKR. At homeostasis, GSN forms a spatial arrangement in which the actin-binding domains are inaccessible. Activation of GSN instigates a conformational change to expose its actin-binding domain. Regulation of GSN has been previously shown to occur through activation from calcium influx or inhibition by PtdIns(4,5)P_2 binding, triggering consequent phosphorylation by protein kinase Cs (PKCs) or pp60$^{c\text{-}src}$. In the absence of detected phosphorylation control by PKR, we propose a unique mechanism whereby PKR affects the cellular cytoskeleton by binding to GSN and sequestering the protein in an inactive conformation away from actin. Accordingly, a truncated GSN with reduced autoinhibition interacted less with PKR. Juxtaposed to this, analysis of direct protein associations demonstrated that increased levels of PKR reduce the association of GSN with actin.

As an expected consequence of the control of GSN by PKR, a number of actin-dependent functions were altered in cells ablated for PKR. This was evident by PKR-deficient fibroblasts having decreased amounts of filamentous actin and reduced rates of actin polymerization compared to WT cells. A reduction in actin stress fibers in PKR-deficient cells is a good indicator of altered lamellipodia and filopodia function and so can be attributed to elevated GSN activity (Hoffmeister et al., 2001; Mazur et al., 2010). Importantly, the altered actin state in PKR-deficient fibroblasts could be rescued by restoring PKR expression or by siRNA knockdown of GSN and these effects in PKR-deficient fibroblasts are antithetical to those in GSN-deficient fibroblasts (Witke et al., 1995). This PKR-dependent control of the actin

state altered basic cellular functions. In keeping with the inhibition of GSN by PKR, ablating PKR in fibroblasts markedly elevated membrane ruffling. In accordance with increased membrane ruffling, PKR-deficient fibroblasts showed increased uptake of dextran sulfate. Together, the data suggest that the inhibition of GSN by PKR could bolster the immune response by limiting pathogen entry into uninfected cells. This scenario was persuasively supported by the demonstration that reduced expression of GSN also reduced entry and production of both herpes virus and rhinovirus in cells.

Hence, our findings suggest a role for GSN in the susceptibility of cells to infection. Viruses and bacteria have been shown to alter the cytoskeleton through regulation of actin-binding proteins, demonstrating the importance of the cellular cytoskeleton during infection (Doceul et al., 2010; McGhie et al., 2004). Previously, GSN was shown to be required for the transport and release of Parvovirus from infected cells (Bär et al., 2008). As stated, reduction of GSN suppressed virus entry into the cell and accordingly reduced virus production and virus-induced cellular death, supporting the concept that GSN is an antiviral target. GSN-regulated processes could also be predicted to be important in formation of the immune synapse, and so PKR could potentially affect processes such as antigen presentation. Potentially relevant to this, PKR-deficient mice have been demonstrated to have delayed development of virus-specific T cells and diminished protective immunity (Nakayama et al., 2010). Unlike cells of the immune system, fibroblasts and some epithelial cells have a high dependency on GSN for regulation of actin during these processes. These effects on the cell suggest that the benefit of the control of GSN by PKR may be in the immune response to intracellular pathogens. It would, therefore, be interesting to measure the effect of PKR on actin remodeling in other cell types, particularly dendritic and T cells.

Unlike GSN, PKR has a well-established role in innate immunity, particularly in protection against viral infection. However, the kinase has not previously been linked to control of the cell cytoskeleton. Other reports have proposed that the innate immune proteins RIG-I and Bcl2 modify the cell cytoskeleton (Ke et al., 2010; Mukherjee et al., 2009). In these instances the proteins directly bind to actin filaments. Although we also found PKR bound to actin, this association did not alter with stimuli that activated PKR and so does not account for the activation-dependent effects of PKR upon actin. Instead, we propose that PKR-dependent modulation of the cytoskeleton appears to be via direct control over the actin-regulatory protein GSN. PKR expression is induced by type I IFNs produced in response to viral infection. Accordingly, we showed that treatment of fibroblasts with IFN-α increased the formation of actin filaments. Importantly, this effect was significant only in WT and not in PKR-deficient fibroblasts. Hence, IFN-mediated effects upon the state of actin in fibroblasts were largely attributable to PKR. This is informative in light of the previously noted RIG-I-dependent effects on the actin cytoskeleton. Therefore, part of the systemic resistance to virus infection induced by IFNs may be attributable to the control of GSN by PKR in uninfected cells. Crucially, we also show that the association between PKR and GSN was disrupted upon activation of PKR and this disruption was ablated in kinase-dead PKR (K296R). Hence, PKR can act as a switch to control GSN, with inhibition of GSN released upon activation of PKR by virus replication.

In summary, PKR associates with GSN to inhibit its activity. This effect occurs at homeostatic condition and is reinforced by IFN (which induces PKR) but is lost upon activation of PKR. As a consequence of this, PKR was shown to alter actin dynamics and accordingly the cell cytoskeleton and dependent processes. Together our data suggest that PKR could bolster resistance to pathogens by altering mechanical features of the cell that limit viral infection. This concept, that innate immunity can regulate actin filament formation, actin-dependent processes in cells, and feed back to innate immunity through membrane ruffling, endocytosis, and viral uptake, is an important advance in our understanding of cell immunity and may have significant implications for the interplay between different cell types that subsequently influence the development of acquired immune resistance. An additional implication of our findings is that the cell cytoskeleton might be targeted as a method of achieving broad antiviral protection.

EXPERIMENTAL PROCEDURES

Cell Treatments

Cells were cultured in Dulbecco's modified Eagle's medium (DMEM) supplemented with 10% fetal bovine serum (FBS) at 37°C in a 5% CO_2 humidified incubator and plated onto either confocal glass coverslips or Fluorodishes (WPI Inc.) for imaging. Prior to visualization of actin filaments, serum (0.05%–1%) was reduced overnight and then removed entirely immediately prior to FRAP experiments. MEFs, HeLa, A549, or HEK293T cells at approximately 40%–60% confluency were transfected with plasmid constructs with Fugene HD/6 (Roche) according to the manufacturer's instructions. Either 100 ng DNA per 12 mm round coverslip in a 24-well plate (BD Falcon) or 200 ng for a 35 mm Fluorodish was transfected. The Venus constructs were transfected in equimolar ratios into cells on glass coverslips. A minimum of 16 hr was given for maturation of a fluorescent signal.

Viral infections were conducted at a multiplicity of infection of between 10 and 100 for either human HSV-1 or HRV-16 in full or 2% serum, respectively. Cells were rinsed with PBS and then fixed in 10% formalin, rinsed again, then permeabilized in 0.1% Triton X-100 in PBS for 5 min. HRV-16 entry into cells was quantitated with the monoclonal antibody against VP2 capsid protein, RV16-7, incubated for 1 hr, followed by the secondary antibody. Virus-infected cells were prelabeled with Celltracker CMRA or Alexa 647 Phalloidin to detect the cell boundary. Viral production was measured 24 hr after infection by titrating the culture supernatant onto L929 cells.

Uptake of dextran particles was visualized in immortalized fibroblast cells allowed to attach overnight prior to reducing the serum levels (1%). Cells were stained with the plasma membrane stain CellMask, according to the manufacturer's protocol, prior to the addition of FITC-labeled 3 kDa dextran particles at a concentration of 25 μg/ml. Cells were fixed after 45 min and imaged as described.

Additional details about the experimental reagents are described in the Supplemental Information.

Fluorescence Microscopy

F- and G-actin was visualized by staining for 30 min with Alexa 488 phalloidin and TRITC-deoxyribonuclease-I according to the manufacturer's guidelines. The F:G-actin ratio was measured in 96-well format on the Cellomics VTi ArrayScan high content screener with the green fluorescein (FITC, 475 ± 40 nm) and red (TRITC, 549 ± 9 nm) channels. Cellular F-actin was visualized by fixing, staining, and mounting on coverslips in Mowiol 4-88 and imaging with the Nikon C1 with GFP (excitation [Ex] 487 nm, emission [Em] 500–530 nm) and TRITC (Ex 547 nm, Em 567–642 nm) channels, as well as on the Applied Precision Deltavision Core System microscope (Semrock, GFP filter set). Particle engulfment or virus infections were similarly imaged as single confocal plane images on the Zeiss LSM 780 by overlapping tile-scanning with a minimum

of 50 fields of view, between 1 and 10 cells per image, or by z stacks collected on the Deltavision Core system. Cells were modeled for the cell edge in Imaris to ensure that the fluorescent signal was internal. All Deltavision images underwent at least 15 rounds of deconvolution with the Deltavision algorithm.

Actin filaments were quantified after staining with phalloidin, as described previously (Yoshigi et al., 2003). Deconvoluted Deltavision images were processed in the Bitplane Imaris software. Built-in surface rendering was used to model actin stress fibers/cell, using the software to exclude actin filaments smaller than 1 μm in width and 2–5 μm in length. The edge of the cell was excluded from calculations. Statistics for average filament length (ellipsoid length), average number of filaments (objects), and total filament volume (sum volume) were exported from the modeled actin stress fiber surfaces. A total of 12 images per cell type (four per coverslip, in triplicate) were modeled and statistics exported.

FRET and FRAP measurements were performed on the Leica SP5 multichannel confocal with a bleach Ex of 40%–50% of a 20 mW laser at 458 (CFP), 514 (Venus), and 561 (RFP) nm to obtain ~50% bleaching. To visualize actin filaments (live cell or recombinant actin), the SP5 was run at 200 mHz, enhanced mode, and 12/16 bit images were taken. FRAP was performed on cells transfected with mRFP1-actin and grown in reduced serum overnight to enhance actin stress fiber formation. Regions of approximately 3 μm were selected on large actin stress fibers. Measurements of fluorescence intensity were then recorded every 2.5628 s for 120 s. Low laser intensity was used for continual measurements to minimize bleaching. Measurements were then normalized to the maximum and minimum intensity (post-bleach point). Data were then accumulated from multiple experiments with multiple regions of interest and up to 50 cells per cell line. FRAP curves were analyzed as per the EMBL FRAP manual (Koti Miura). Individual one-phase exponential association curves were also plotted in Graphpad Prism software and the $t_{1/2}$ times of curves with an R^2 value of greater than 0.25 and an SD of <5 were recorded. The majority of PKR-deficient and Bac10 cells did not reach significant recovery after bleaching to model regression curves. The minimum number of filaments, after thresholds, per time point for any cell type was 18, with a maximum of 65.

Acceptor photobleaching FRET was performed between GSN-CFP or GSNCT-CFP and PKR-Venus, or actin-mRFP1/actin-eYFP. Photobleaching was optimized to reduce the fluorescent signal after bleaching to approximately 50% of the original intensity. FRET efficiencies were calculated with the inbuilt software (Leica LAS Advanced Fluorescence). Images were acquired sequentially with averaging, and donor/acceptor-only controls were utilized to ensure no spectral overlap. FLIM experiments were conducted with a lifetime imaging attachment (Lambert Instruments) mounted on an inverted microscope (TE2000U, Nikon Inc, Japan), as described previously (Clayton et al., 2005). Fixed cells were excited with epi-illumination with a modulated 455 nm LED at 40 MHz and observed with a 100× NA 1.25 oil objective (Nikon Plan-Fluor) through a filter set designed for CFP (Nikon, EX430-450, DM455, BA465-495) or FITC (Nikon FITC, DM505, Em 515–555 nm). The mean extent of lifetime quenching was estimated from the mean fluorescence lifetime (mean of the phase and modulation lifetimes) of the cells in the absence or presence of an acceptor. Average lifetime from >25 single cells is plotted on an AB plot, as described previously (Clayton et al., 2004), to demonstrate lifetime shortening of FRET in the presence of acceptor. CFP/GFP controls were used to ensure that the lifetime of fusion proteins resembled that of individual fluorophores.

Split Venus experiments were imaged on the Leica SP5 multichannel under eYFP conditions and on a Nikon C1 confocal (GFP settings).

Actin polymerization assays were performed with rhodamine-labeled actin monomers prepared at 5 μM and incubated with or without 0.5 μM GSN1-6, GSN3-4, PKR, and K296R-PKR in polymerization buffer and used as previously published (Yin et al., 1980, 1981). The reaction was mixed and spotted onto 12 mm coverslips for 90 min at room temperature prior to mounting in Mowiol 4-88. Actin polymers were visualized by the tile-scanning module within the Leica LAS AF software and collecting continuous images in a 3 × 5 grid. Images were quantified in NIH Image J by mean fluorescence intensity of the entire field of view.

In Vivo Experiments

Intranasal inhalation was used to deliver recombinant lentivirus and adenovirus into the lung of 6- to 12-week-old C57BL6/J mice according to a previously published protocol (DuPage et al., 2009). Lentiviruses containing control (SHC001) or GSN-targeting (SHCLNG-NM_146120) shRNAs were generated according to the manufacturer's instructions (Sigma) and infected at 1×10^5 MOI for 3 days to reduce levels of GSN in the mouse airway epithelia. Subsequent infection with an MOI of 5×10^6 Adeno-β-Gal-GFP (Gene Transfer Vector Core) was used to identify differences in viral uptake into the lung. After 4–5 days, lungs were removed and processed (according to DuPage et al., 2009). GSN was quantitated by immunostaining with the N-18 (Santa Cruz) primary and Alexa 647 secondary antibodies. β-gal was detected by immunostaining with the ZBG1 (Zymed) primary and Dylight 594 (AbCam) secondary antibodies, as well as by color conversion of X-gal. RGB merged images were collected under transmitted light and immunostaining collected under fluorescence imaging on the Deltavision (with predominantly Far-Red/Cy5 filters to minimize autofluorescence). All mice used in experiments were treated according to practices approved by the Monash University Animal Ethics Committee as obligated by the Australian Code of Practice for the Care and Use of Animals for Scientific Purposes, in compliance with standards mandated by the National Health and Medical Research Council and National Institutes of Health.

Statistics

Unless otherwise stated, all statistics were performed with the GraphPad Prism software and displayed as the mean and SEM. If not otherwise stated in the figure legends, all significance analyses were two-tailed, unpaired, Student t tests comparing two sets of data. *$p < 0.05$; **$0.05 \geq p \geq 0.001$; ***$p < 0.001$; ns, not significant.

SUPPLEMENTAL INFORMATION

Supplemental Information includes Supplemental Experimental Procedures, five figures, and four movies and can be found with this article online at doi:10.1016/j.immuni.2012.02.020.

ACKNOWLEDGMENTS

We would like to thank F. Cribbin for editorial assistance in preparing this manuscript, C. Lo for assistance in preparing image data, M. Kinter for mass spectrometry, J. Bamburg for fluorescent actin constructs, S. Michnick and J.-F. Paradis for split Venus plasmids, and P. Faber for genetic constructs. We are also very grateful to N. De Weerd and P. Hertzog for purified recombinant IFN-α, B. Thomas and P. Bardin for the HRV-16, N. McMillan for the HSV-1 isolate, F. Carbone for the GFP HSV-1 isolate, M. Behlke (Integrated DNA Technologies) for the siRNA targeting GSN, and N. Watkins for the recombinant adenovirus and procedures to use this virus in vivo. This work was supported by the Victorian Government's Operational Infrastructure Support Program and by an NIH grant (R01AI034039) to B.R.G.W.

Received: May 17, 2011
Revised: December 30, 2011
Accepted: February 29, 2012
Published online: May 24, 2012

REFERENCES

Aidinis, V., Carninci, P., Armaka, M., Witke, W., Harokopos, V., Pavelka, N., Koczan, D., Argyropoulos, C., Thwin, M.M., Möller, S., et al. (2005). Cytoskeletal rearrangements in synovial fibroblasts as a novel pathophysiological determinant of modeled rheumatoid arthritis. PLoS Genet. *1*, e48.

Arora, P.D., Chan, M.W., Anderson, R.A., Janmey, P.A., and McCulloch, C.A. (2005). Separate functions of gelsolin mediate sequential steps of collagen phagocytosis. Mol. Biol. Cell *16*, 5175–5190.

Asch, H.L., Head, K., Dong, Y., Natoli, F., Winston, J.S., Connolly, J.L., and Asch, B.B. (1996). Widespread loss of gelsolin in breast cancers of humans, mice, and rats. Cancer Res. *56*, 4841–4845.

Bär, S., Daeffler, L., Rommelaere, J., and Nüesch, J.P. (2008). Vesicular egress of non-enveloped lytic parvoviruses depends on gelsolin functioning. PLoS Pathog. *4*, e1000126.

Burtnick, L.D., Koepf, E.K., Grimes, J., Jones, E.Y., Stuart, D.I., McLaughlin, P.J., and Robinson, R.C. (1997). The crystal structure of plasma gelsolin: implications for actin severing, capping, and nucleation. Cell *90*, 661–670.

Campbell, J.J., and Knight, M.M. (2007). An improved confocal FRAP technique for the measurement of long-term actin dynamics in individual stress fibers. Microsc. Res. Tech. *70*, 1034–1040.

Chellaiah, M., Kizer, N., Silva, M., Alvarez, U., Kwiatkowski, D., and Hruska, K.A. (2000). Gelsolin deficiency blocks podosome assembly and produces increased bone mass and strength. J. Cell Biol. *148*, 665–678.

Clayton, A.H., Hanley, Q.S., and Verveer, P.J. (2004). Graphical representation and multicomponent analysis of single-frequency fluorescence lifetime imaging microscopy data. J. Microsc. *213*, 1–5.

Clayton, A.H., Walker, F., Orchard, S.G., Henderson, C., Fuchs, D., Rothacker, J., Nice, E.C., and Burgess, A.W. (2005). Ligand-induced dimer-tetramer transition during the activation of the cell surface epidermal growth factor receptor-A multidimensional microscopy analysis. J. Biol. Chem. *280*, 30392–30399.

Crowley, M.R., Head, K.L., Kwiatkowski, D.J., Asch, H.L., and Asch, B.B. (2000). The mouse mammary gland requires the actin-binding protein gelsolin for proper ductal morphogenesis. Dev. Biol. *225*, 407–423.

De Corte, V., Gettemans, J., and Vandekerckhove, J. (1997). Phosphatidylinositol 4,5-bisphosphate specifically stimulates PP60(c-src) catalyzed phosphorylation of gelsolin and related actin-binding proteins. FEBS Lett. *401*, 191–196.

Dey, M., Cao, C., Dar, A.C., Tamura, T., Ozato, K., Sicheri, F., and Dever, T.E. (2005). Mechanistic link between PKR dimerization, autophosphorylation, and eIF2alpha substrate recognition. Cell *122*, 901–913.

Doceul, V., Hollinshead, M., van der Linden, L., and Smith, G.L. (2010). Repulsion of superinfecting virions: a mechanism for rapid virus spread. Science *327*, 873–876.

dos Remedios, C.G., Chhabra, D., Kekic, M., Dedova, I.V., Tsubakihara, M., Berry, D.A., and Nosworthy, N.J. (2003). Actin binding proteins: regulation of cytoskeletal microfilaments. Physiol. Rev. *83*, 433–473.

DuPage, M., Dooley, A.L., and Jacks, T. (2009). Conditional mouse lung cancer models using adenoviral or lentiviral delivery of Cre recombinase. Nat. Protoc. *4*, 1064–1072.

Ferjani, I., Fattoum, A., Maciver, S.K., Bénistant, C., Chahinian, A., Manai, M., Benyamin, Y., and Roustan, C. (2006). A direct interaction with calponin inhibits the actin-nucleating activity of gelsolin. Biochem. J. *396*, 461–468.

Furukawa, K., Fu, W., Li, Y., Witke, W., Kwiatkowski, D.J., and Mattson, M.P. (1997). The actin-severing protein gelsolin modulates calcium channel and NMDA receptor activities and vulnerability to excitotoxicity in hippocampal neurons. J. Neurosci. *17*, 8178–8186.

Groves, E., Dart, A.E., Covarelli, V., and Caron, E. (2008). Molecular mechanisms of phagocytic uptake in mammalian cells. Cell. Mol. Life Sci. *65*, 1957–1976.

Halavatyi, A.A., Nazarov, P.V., Medves, S., van Troys, M., Ampe, C., Yatskou, M., and Friederich, E. (2009). An integrative simulation model linking major biochemical reactions of actin-polymerization to structural properties of actin filaments. Biophys. Chem. *140*, 24–34.

Hedberg, K.M., Bengtsson, T., Safiejko-Mroczka, B., Bell, P.B., and Lindroth, M. (1993). PDGF and neomycin induce similar changes in the actin cytoskeleton in human fibroblasts. Cell Motil. Cytoskeleton *24*, 139–149.

Hoffmeister, K.M., Falet, H., Toker, A., Barkalow, K.L., Stossel, T.P., and Hartwig, J.H. (2001). Mechanisms of cold-induced platelet actin assembly. J. Biol. Chem. *276*, 24751–24759.

Ke, H., Parron, V.I., Reece, J., Zhang, J.Y., Akiyama, S.K., and French, J.E. (2010). BCL2 inhibits cell adhesion, spreading, and motility by enhancing actin polymerization. Cell Res. *20*, 458–469.

Leib, D.A., Machalek, M.A., Williams, B.R., Silverman, R.H., and Virgin, H.W. (2000). Specific phenotypic restoration of an attenuated virus by knockout of a host resistance gene. Proc. Natl. Acad. Sci. USA *97*, 6097–6101.

Lin, K.M., Wenegieme, E., Lu, P.J., Chen, C.S., and Yin, H.L. (1997). Gelsolin binding to phosphatidylinositol 4,5-bisphosphate is modulated by calcium and pH. J. Biol. Chem. *272*, 20443–20450.

Lu, M., Witke, W., Kwiatkowski, D.J., and Kosik, K.S. (1997). Delayed retraction of filopodia in gelsolin null mice. J. Cell Biol. *138*, 1279–1287.

Maury, C.P., Alli, K., and Baumann, M. (1990). Finnish hereditary amyloidosis. Amino acid sequence homology between the amyloid fibril protein and human plasma gelsoline. FEBS Lett. *260*, 85–87.

Mazur, A.J., Gremm, D., Dansranjavin, T., Litwin, M., Jockusch, B.M., Wegner, A., Weeds, A.G., and Mannherz, H.G. (2010). Modulation of actin filament dynamics by actin-binding proteins residing in lamellipodia. Eur. J. Cell Biol. *89*, 402–413.

McGhie, E.J., Hayward, R.D., and Koronakis, V. (2004). Control of actin turnover by a salmonella invasion protein. Mol. Cell *13*, 497–510.

Mukherjee, A., Morosky, S.A., Shen, L., Weber, C.R., Turner, J.R., Kim, K.S., Wang, T., and Coyne, C.B. (2009). Retinoic acid-induced gene-1 (RIG-I) associates with the actin cytoskeleton via caspase activation and recruitment domain-dependent interactions. J. Biol. Chem. *284*, 6486–6494.

Nakayama, Y., Plisch, E.H., Sullivan, J., Thomas, C., Czuprynski, C.J., Williams, B.R., and Suresh, M. (2010). Role of PKR and Type I IFNs in viral control during primary and secondary infection. PLoS Pathog. *6*, e1000966.

Nobile, C., Rudnicka, D., Hasan, M., Aulner, N., Porrot, F., Machu, C., Renaud, O., Prévost, M.C., Hivroz, C., Schwartz, O., and Sol-Foulon, N. (2010). HIV-1 Nef inhibits ruffles, induces filopodia, and modulates migration of infected lymphocytes. J. Virol. *84*, 2282–2293.

Sadler, A.J., Latchoumanin, O., Hawkes, D., Mak, J., and Williams, B.R. (2009). An antiviral response directed by PKR phosphorylation of the RNA helicase A. PLoS Pathog. *5*, e1000311.

Safiejko-Mroczka, B., and Bell, P.B., Jr. (2001). Reorganization of the actin cytoskeleton in the protruding lamellae of human fibroblasts. Cell Motil. Cytoskeleton *50*, 13–32.

Sun, H.Q., Kwiatkowska, K., Wooten, D.C., and Yin, H.L. (1995). Effects of CapG overexpression on agonist-induced motility and second messenger generation. J. Cell Biol. *129*, 147–156.

Sun, H., Lin, K., and Yin, H.L. (1997). Gelsolin modulates phospholipase C activity in vivo through phospholipid binding. J. Cell Biol. *138*, 811–820.

Wang, T., Chuang, T.-H., Ronni, T., Gu, S., Du, Y.-C., Cai, H., Sun, H.-Q., Yin, H.L., and Chen, X. (2006). Flightless I homolog negatively modulates the TLR pathway. J. Immunol. *176*, 1355–1362.

Witke, W., Sharpe, A.H., Hartwig, J.H., Azuma, T., Stossel, T.P., and Kwiatkowski, D.J. (1995). Hemostatic, inflammatory, and fibroblast responses are blunted in mice lacking gelsolin. Cell *81*, 41–51.

Yin, H.L., Zaner, K.S., and Stossel, T.P. (1980). Ca2+ control of actin gelation. Interaction of gelsolin with actin filaments and regulation of actin gelation. J. Biol. Chem. *255*, 9494–9500.

Yin, H.L., Hartwig, J.H., Maruyama, K., and Stossel, T.P. (1981). Ca2+ control of actin filament length. Effects of macrophage gelsolin on actin polymerization. J. Biol. Chem. *256*, 9693–9697.

Yoshigi, M., Clark, E.B., and Yost, H.J. (2003). Quantification of stretch-induced cytoskeletal remodeling in vascular endothelial cells by image processing. Cytometry A *55*, 109–118.

MCB Accepts, published online ahead of print on 14 May 2012
Mol. Cell. Biol. doi:10.1128/MCB.00310-12

Regulatory effects of programmed cell death 4 (PDCD4) protein in ISG expression and generation of Type I IFN-responses

Barbara Kroczynska◆, Bhumika Sharma◆, Elizabeth A. Eklund◆, Eleanor N. Fish¶ and Leonidas C. Platanias◆*

◆Robert H. Lurie Comprehensive Cancer Center and Division of Hematology-Oncology, Northwestern University Medical School and Jesse Brown Veterans Affairs Medical Center, Chicago, IL

¶ Toronto Research Institute, University Health Network and Department of Immunology, University of Toronto, Toronto, ON M5G 2M1, Canada

Running Title: IFNR-mediated regulation of PDCD4 and its role in IFN-responses

* Address correspondence to: Leonidas C. Platanias, Robert H. Lurie Comprehensive Cancer Center, 303 East Superior Street, Lurie 3-107, Chicago, IL 60611, Tel. 312-503-4267; Fax. 312-908-1372, Email: l-platanias@northwestern.edu

Abstract

The precise mechanisms by which the activation of IFN receptors (IFNRs) ultimately controls mRNA translation of specific target genes to induce IFN-dependent biological responses remain ill-defined. We provide evidence that IFNα induces phosphorylation of programmed cell death 4 (PDCD4) protein on Ser67. This IFNα-dependent phosphorylation is mediated by either the p70 S6 kinase (S6K) or the p90 ribosomal protein S6K (RSK) in a cell type-specific manner. IFN-dependent phosphorylation of PDCD4 results in down regulation of PDCD4 protein levels, as the phosphorylated form of PDCD4 interacts with the ubiquitin ligase βTRCP and undergoes degradation. This process facilitates IFN-induced eukaryotic translation initiation factor 4A (eIF4A) activity and binding to translation initiation factor eIF4G to promote mRNA translation. Our data establish that PDCD4 degradation ultimately facilitates expression of several ISG protein products that play important roles in the generation of IFN-responses, including ISG15, $p21^{WAF1/CIP1}$, and SLFN5. Moreover, engagement of the RSK/PDCD4 pathway by the Type I IFNR is required for the suppressive effects of IFNα on normal CD34+ hematopoietic precursors and antileukemic effects *in vitro*. Altogether, these findings provide evidence for a unique function of PDCD4 in the Type I IFN system and indicate a key regulatory role for this protein in mRNA translation of ISGs and control of IFN responses.

Introduction

Interferons (IFNs) are a family of pleiotropic cytokines that inhibit viral replication and exhibit important immunomodulatory, antiproliferative and antitumor properties via their regulatory effects on cell cycle progression, cell proliferation and, under certain circumstances, apoptosis (5, 35, 47). Because of these activities, IFNs have been examined extensively in clinical trials over the last 3 decades and have found applications in the management of various malignancies, viral syndromes and autoimmune disorders (35, 49, 57, 59). This broad spectrum of clinical applications for IFNs is a reflection of the diversity of their biological effects.

There are three major IFN groups/families: Type I (α, β, ε, κ and ω), Type II (γ), and Type III (λ) (8, 35, 47). The mechanisms by which IFNs initiate transcription of target genes have been excessively studied and precisely defined over the years. Engagement of IFN receptors (IFNRs) activate Janus kinase (JAK)-signal transducer and activator of transcription (STAT) signaling pathways, leading to transcriptional induction of IFN-stimulated genes (ISGs) and ultimately the generation of ISG products which are critical in order for the IFN-biological responses to occur (6, 29, 39, 47). Notably, distinct combinations of JAKs at the receptor complex and inducible STAT-complexes are differentially regulated by different types of IFNs, allowing for gene expression specificity via distinct STAT-binding elements in the promoters of ISGs (6, 8, 29, 30, 39, 43, 47).

In previous work we provided evidence that the AKT/mTOR pathway is activated during engagement of IFNRs and regulates downstream engagement of various effectors of the pathway, including S6K/rpS6, 4E-BP1 and eIF4B (19, 20, 22, 23, 27, 28).

Moreover, we demonstrated that the functions of AKT and the PI3'K pathway upstream of AKT are essential for engagement of IFN-regulated mTOR effector elements and initiation of mRNA translation of certain ISGs (20, 21).

PDCD4 is a translational repressor that blocks the eIF4A helicase activity by binding to eIF4A and also interfering with eIF4A binding to eIF4G, resulting in negative effects/control on the initiation of mRNA translation (25, 37, 48, 55). Recent studies have shown a function for PDCD4 as a tumor suppressor that is lost in certain aggressive malignant diseases (11, 12, 24, 31, 33, 44). Interestingly, emerging evidence also suggests that the function of PDCD4 can be altered by the co-factor protein arginine methyltransferase 5 (PRMT5) and that arginine methylation of PDCD4 results in acceleration of tumor growth (41). Thus, there is accumulating evidence that PDCD4 plays an important role in the control of tumorigenesis and its deregulation has important consequences in cell proliferation and neoplastic transformation.

In the present study we examined whether engagement of the Type I IFNR results in modulation of PDCD4 phosphorylation and assessed the effects of Type I IFN-treatment on the levels of PDCD4 protein expression. Our studies provide evidence that IFN-dependent phosphorylation of PDCD4 on serine 67 results in enhanced interaction of PDCD4 with βTRCP (β-transducin repeat-containing protein), and this is followed by PDCD4 degradation. We also demonstrate that the activity of the S6 kinase (S6K) is required for phosphorylation of PDCD4 in mouse embryonic fibroblasts (MEFs), while RSK1 is the kinase responsible for this phosphorylation in U266 and KT1 hematopoietic cells. Our data also demonstrate that pharmacological inhibitor of RSK, or siRNA-mediated RSK1 knockdown, results in blocking of IFNα -inducible expression of ISG15,

105 p21$^{WAF1/CIP1}$, and Schlafen 5 (SLFN5), and results in partial reversal of the
106 antiproliferative effects of IFNα. Altogether, our data provide the first direct evidence
107 implicating PDCD4 in IFN-signaling and suggest a key regulatory role for the
108 RSK/PDCD4 pathway in the generation of the biological properties of Type I IFNs.
109
110
111
112
113
114
115
116
117
118
119
120
121
122
123
124

Materials and Methods

Cells and Reagents The human KT1 and U266 cell lines were grown in RPMI 1640 medium supplemented with 10% fetal bovine serum (FBS) and antibiotics. In some experiments, the cells were serum-starved for 24 hours, prior to the indicated treatments. Immortalized S6K1/2+/+ and S6K1/2-/- MEF cells (38) were grown in or DMEM medium supplemented with 10% and antibiotics. In some experiments, the MEF cells were serum-starved in 0.5% FBS for 24 hours, prior to the indicated treatments. Antibodies against, $p21^{Waf1/Cip1}$ and against the phosphorylated form of PDCD4 , and RSK1 were purchased from Abcam (Cambridge, MA). An antibody against PDCD4 were purchased from Rockland (Gilbertsville, PA). Antibodies against eIF4A, βTRCP, PDCD4 were obtained from Santa Cruz Biotechnology (Santa Cruz, CA) and were used in immunoprecipitations. Control siRNA, siRNA targeting PDCD4 or RSK1, control shRNA, shRNA targeting PDCD4, and puromycin were from Santa Cruz Biotechnology (Santa Cruz, CA). An antibody against SLFN5 was obtained from Sigma Aldrich (Steinheim, Germany). A monoclonal antibody recognizing human ISG15 was kindly provided by Dr. Ernest Borden (Taussing Cancer Center, Cleveland). An antibody against GAPDH was from Chemicon (Billerica, MA). Antibodies against phospho-Thr202/Tyr204-ERK1/2, ERK1/2, phospho-Ser221-RSK1, RSK1, phospho-Thr421/Ser424-p70S6K, anti-p70S6K, phospho-Ser240/244-rpS6, rpS6, eIF4A, eIF4E, eIF4G, 4E-BP1, HA were obtained from Cell Signaling Technology (Beverly, MA). Normal CD34+ bone-marrow derived cells were obtained from Lonza (Basel, Switzerland). Recombinant human IFNα was provided by Hoffman La Roche, Inc. The FRAP/mTOR inhibitor, rapamycin and the MEK1/2 inhibitor U0126, the proteosomal

inhibitor MG-132, phosphatase, and protease inhibitor were obtained from Calbiochem Inc. (La Jolla, CA). The RSK inhibitor SL0101-1-1 was from Symansis (Auckland, New Zealand). 7-Methyl GTP-Sepharose was from GE Healthcare UK Limited (Little Chalfont Buckinghamshire, UK). The siRNA transfection reagent TransIT-TKO, and plasmid DNA transfection reagent TransIT-LT1 was from Mirus Bio Corporation (Madison, WI). Nucleofector solution was from Lonza Cologne AG (Cologne, Germany). Recombinant PDCD4 protein was from Prospec (Rehovot, Israel). Clean-Blot IP detection reagent was from Thermo Scientific. HA-tagged wild type PDCD4 or HA-tagged PDCD4 (S67/71A) (10) were a gift from Dr. Michele Pagano (Department of Pathology, New York University).

Immunoprecipitations and Immunoblotting Cells were treated with IFNα for the indicated times and lysed in phosphorylation lysis buffer (PLB) as in previous studies (19-23). Cells were serum starved for 24 hours prior to the indicated treatments. Immunoprecipitations and immunoblotting using an enhanced chemiluminescence (ECL) method were performed as previously described (19-23). In some experiments the cells were pre-incubated with rapamycin (20 nM) or U0126 (10 μM) for 60 minutes or SL0101-1 (60 μM) for 3 hours prior to IFN-treatment.

Cap Binding assays These studies were performed as previously described (22). Briefly, KT1 cells were incubated for 24 hours in serum-free medium and then pre-treated for 60 minutes with rapamycin (20 nM) or SL0101-1 (60 μM), followed by IFNα-treatment for the indicated times. Cell lysates were incubated with 7-methyl-GTP Sepharose

(Amersham) for 4 hours and then washed with lysis buffer. Proteins were resolved by SDS-PAGE electrophoresis, transferred onto immobilon (Millipore), and probed with the indicated antibodies.

In vitro kinase assays Immune complex kinase assays to detect RSK1 kinase activity in anti-RSK1 immunoprecipitates were performed essentially as previously described (23). PDCD4 was used as an exogenous substrate.

Isolation of polysomal RNA and quantitative RT-PCR KT1 cells transduced with control shRNA or shRNA targeting human PDCD4 were serum starved for 24 hours and then left untreated or treated with IFN-α for 24 hours. Isolation of polysomal RNA and quantitative RT-PCR on the polysomal fractions were performed as previously described (16). Real-time PCR for the *Isg15*, *p21* and *slfn5* genes was conducted using commercially available FAM-labeled probes and primers (Applied Biosystems), and *gapdh* was used for normalization. mRNA amplification was determined as previously described (15, 16), and relative quantitation of mRNA levels was plotted as fold increase as compared to untreated samples.

Hematopoietic progenitor assays in methylcellulose Clonogenic assays in methyl-cellulose, to detect leukemic CFU-blast (CFU-L) colony formation from KT1 cells were performed essentially as previously described (4). The effects of IFNα on CFU-L colony formation from KT1 cells transfected with control siRNA or siRNAs specific for PDCD4 or HA-tagged PDCD4 (S67/71A) were performed essentially as previously described (4).

Myeloid progenitor (CFU-GM) colony formation from normal CD34+ cells was assessed in clonogenic assays in methylcellulose, as previously described (45).

Results

There is evidence that PDCD4 is a target for the kinase activity of S6K in other systems (9) and our previous work has demonstrated that S6K is phosphorylated/ activated in a Type I IFN-dependent manner in different cell types (23, 28, 36). We examined whether IFNα induces phosphorylation of PDCD4 and, if so, whether such phosphorylation occurs in an S6K-dependent manner. For this purpose, experiments were performed using immortalized MEFs with targeted disruption of both the *S6k1* and *S6k2* genes (38). Serum-starved MEFs were incubated in the presence or absence of mouse IFNα and total cell lysates were resolved by sodium dodecyl sulfate-polyacrylamide gel electrophoresis (SDS-PAGE) and immunoblotted with an antibody against the phosphorylated form of PDCD4 on serine 67. IFNα-treatment resulted in induction of phosphorylation of PDCD4 on Ser67 in S6k1+/+S6k2+/+ MEFs, but this phosphorylation was defective in S6k1/S6k2 double-knockout MEFs (Fig. 1A). Notably, when wild-type MEFs were pre-incubated with the mTOR inhibitor rapamycin, the phosphorylation of PDCD4 on Ser67 was blocked (Fig.1B), consistent with the lack of phosphorylation seen in the S6k1/S6k2 double-knockout MEFs. On the other hand, IFNα-dependent PDCD4 phosphorylation was still detectable in cells treated with the MEK inhibitor U0126 (Fig. 1B).

PDCD4 phosphorylation on Ser67 results in the degradation of the protein via the ubiquitin ligase βTRCP, as reported in other systems (9, 10). Accordingly, we examined the effects of IFNα on PDCD4 protein expression in the S6K1/2 double knockout cells. Serum starved S6k1+/+ S6k2+/+ or S6k1-/-S6k2-/- MEFs were treated with IFNα for 6 hours and PDCD4 expression was assessed. After 6 hours of IFN-treatment, detectable

PDCD4 protein levels decreased in S6k1+/+S6k2+/+ MEFs, while they remained unchanged in S6k1-/-S6k2-/- cells (Fig. 1C). Similarly, pre-treatment of the cells with rapamycin, which blocks PDCD4 phosphorylation, reversed the IFNα-dependent decrease in PDCD4 expression (Fig. 1D). In contrast, the addition of the MEK inhibitor U0126 did not reverse these suppressive effects of IFNα (Fig. 1D). It should be noted that the down regulation of PDCD4 was time-dependent, commencing after 120 min of IFN-treatment and reaching a maximum at 180 min (Fig. 1E). To directly examine whether the decrease in protein levels seen after IFN-treatment reflects degradation of the protein, the effects of the proteasomal inhibitor MG132 were assessed. MG132-treatment of the cells resulted in reversal of the IFNα-dependent suppression of PDCD4 (Fig. 1E), suggesting a mechanism involving proteasomal degradation. Altogether, these studies establish that IFNα-induces S6K-mediated phosphorylation of PDCD4 and that this phosphorylation ultimately promotes degradation of PDCD4 protein.

To further define the mechanisms of the IFN-dependent regulation of PDCD4 phosphorylation, similar studies were performed in cells of hematopoietic origin. In previous work we have shown that IFN-inducible phosphorylation of the mTORC1 effector eIF4B is differentially regulated by p706SK or RSK in a cell-type specific manner, with RSK1 being the predominant kinase in cells of hematopoietic origin (23). As there is also evidence by others that RSK and p70S6K can phosphorylate substrates at the RxRxxS/T motif (26, 32, 52), we examined whether PDCD4 phosphorylation can be regulated in hematopoietic cells by RSK, whose activation in the IFN-system is MEK/ERK-dependent (23). As shown in Fig. 2A, IFNα-dependent phosphorylation of PDCD4 and ERK in KT1 cells was blocked by the MEK inhibitor U0126 (Fig. 2A),

263 which regulates upstream IFN-dependent engagement of RSK1 in these cells. Next, the
264 effects of RSK inhibition on IFN-dependent phosphorylation of PDCD4 and
265 downregulation of PDCD4 protein levels were determined in these cells. When KT1
266 cells were treated with the RSK1 inhibitor SL0101-1 we found that phosphorylation of
267 PDCD4 on Ser67 and phosphorylation of RSK1 on Ser221 were blocked (Fig. 2B), while
268 phosphorylation of p70S6K and rpS6 were not (Fig. 2B). Addition of the RSK inhibitor,
269 but not rapamycin, also prevented the decrease in PDCD4 protein levels seen in these
270 cells after prolonged IFN-treatment (Fig. 2C). Similar results were obtained when studies
271 were performed using the U266 hematopoietic cell line. As in the case of KT1 cells,
272 IFNα also induced phosphorylation of PDCD4, and this phosphorylation was SL0101-1-
273 sensitive, but rapamycin-insensitive (Fig. 2D). In addition, the suppression of PDCD4
274 protein levels seen after IFN-treatment was reversible by concomitant SL0101-1
275 treatment of cells (Fig. 2E).

276 To further define the involvement of RSK1 in PDCD4 phosphorylation in
277 hematopoietic cells, experiments were carried out in which RSK1was knocked down in
278 KT1 cells. As shown in Fig. 3A, siRNA-mediated inhibition of RSK1 expression
279 blocked PDCD4 phosphorylation, indicating that in these cells IFNα-induced RSK1 is
280 the dominant kinase controlling PDCD4 phosphorylation (Fig. 3A). In studies in which
281 immune complex kinase assays were conducted on anti-RSK immunoprecipitates, using
282 PDCD4 as an exogenous substrate, we found strong IFNα-inducible phosphorylation of
283 PDCD4, which was blocked by SL0101-1, suggesting that PDCD4 is a substrate for the
284 kinase activity of RSK1 (Fig. 3B).

Previous studies have suggested a model in which after undergoing S6K-mediated phosphorylation on Ser67, PDCD4 interacts with the ubiquitin ligase βTRCP and undergoes proteolytic degradation (9, 10). To determine whether IFN-treatment results in the formation of βTRCP/PDCD4 complexes, co-immunoprecipitation experiments were carried out. Serum starved KT1 cells were treated with IFNα in the presence or absence of SL0101-1 and lysates were immunoprecipitated with an anti-βTRCP antibody, followed by immunoblotting with an antibody against PDCD4. As shown in Fig. 4A, IFNα-treatment induced an association of βTRCP with PDCD4 (Fig. 4A). This IFNα-dependent βTRCP/PDCD4 interaction was not detectable in cells pre-treated with the RSK inhibitor, or in cells transfected with siRNA targeting RSK1 (Fig. 4B). In parallel studies, we examined whether IFN-dependent phosphorylation of PDCD4 modulates its interaction with eIF4A. Cells were treated with IFNα, in the presence or absence of SL0101-1, lysates were immunoprecipitated with an anti-eIF4A antibody and immunoblotted with an anti-PDCD4 antibody. IFNα-treatment resulted in decreased amounts of detectable PDCD4 in association with eIF4A, but this decrease was reversed by treatment of cells with SL0101-1 (Fig. 4C). IFNα- treatment resulted in a significant increase in the amount of eIF4G interacting with eIF4A, but the association was suppressed by treatment of cells with SL0101-1 (Fig. 4C), suggesting involvement for RSK1 activity in the process. In other studies, lysates from cells transfected with control siRNA, or siRNA specifically targeting RSK1, were immunoprecipitated with an anti-eIF4A antibody and immunobloted with anti-PDCD4, anti-eIF4G or anti-eIF4A antibodies (Fig. 4D). IFNα treatment did not decrease the amount of PDCD4 associated with eIF4A in cells in which RSK1 was knocked down (Fig. 4D, E).

As the recruitment of eIF4F to the 5' cap structure of mRNA is an important step in the translation-initiation process, we sought to determine the regulatory effects of IFNα-dependent engagement of RSK and mTOR pathways in KT1 cells on binding of the translation initiation factors to the 7-methylguanosine cap complex. Cells were pre-treated with rapamycin or SL0101-1 and the IFN-inducible recruitment of eIF4G and eIF4A to the complex was assessed. IFNα- inducible binding of eIF4G, eIF4A and eIF4E was clearly detectable (Fig. 5A). As expected, there was no dissociation of unphoshorylated 4E-BP1 in rapamycin-pretreated cell lysates, leading to decreased levels of eIF4G and eIF4A in the complex, reflecting decreased eIF4E binding to eIF4G and associated eIF4A. Interestingly, in cells pre-treated with RSK inhibitor there was normal 4E-BP1 dissociation, but also decreased levels of eIF4A and eIF4G in the complex as compared to cells not pre-treated with the inhibitor (Fig. 5A). Similarly, in experiments in which RSK1 was knocked down (Fig. 5B), we found reversal of IFN-dependent enhanced binding of eIF4G, eIF4A and eIF4E to the 7-methyguanosine cap complex (Fig. 5C), raising the possibility that phosphorylation of PDCD4 mediated by RSK1 increases IFN-inducible eIF4F assembly. To further define the potential role of PDCD4 in the process, we used lysates from cells transfected with control siRNA or siRNA specifically targeting PDCD4 (Fig. 5D). IFNα-treatment resulted in enhanced binding of eIF4G, eIF4A and eIF4E to the 7-methyguanosine cap complex (Fig. 5E), but knockdown of PDCD4 further increased eIF4G, eIF4A and eIF4E binding. Moreover, ectopic expression of a PDCD4 S67/71A mutant (Fig. 5F), which cannot undergo phosphorylation at Ser67 and subsequent degradation (9), decreased the binding of eIF4A and eIF4G to the 5' cap complex (Fig. 5G).

To further delineate the involvement of PDCD4 in eIF4F complex formation, co-immunoprecipitation experiments were carried out. Serum starved KT1 cells were treated with IFNα in the presence or absence of SL0101-1 and lysates were immunoprecipitated with an anti-eIF4E antibody, followed by immunoblotting with antibodies against eIF4G, eIF4A, and eIF4E. As shown in Fig. 5H, IFNα-treatment induced an association of eIF4E with eIF4G and eIF4A. This IFN-dependent interaction was less pronounced in cells pre-treated with SL0101-1 (Fig. 5H). We also performed similar analyses using lysates from cells transfected with control siRNA or siRNA specifically targeting RSK1. As expected, IFNα-treatment resulted in enhanced binding of eIF4G and eIF4A with eIF4E in lysates from cells transfected with control siRNA, but knockdown of RSK1 decreased the amount of eIF4G and eIF4A binding to the eIF4E (Fig. 5I). Consistent with a role for PDCD4 downstream of RSK1 in the process, IFNα-treatment resulted in enhanced binding of eIF4G and eIF4A with eIF4E, but knockdown of PDCD4 further increased the amount of eIF4G and eIF4A binding to the eIF4E (Fig. 5J). On the other hand, there was no effect on the dissociation of 4E-BP1 from eIF4E in cells treated with IFNα, suggesting that PDCD4 exhibits negative effects in IFN-inducible eIF4F complex formation in a 4E-BP1-independent manner (Fig. 5J). Consistent with these findings, ectopic expression of a PDCD4 S67/71A mutant, also decreased the association of eIF4G and eIF4A with eIF4E (Fig. 5K).

As our data suggested a negative regulatory effect of PDCD4 on IFNα - activated eIF4F complexes, likely via inhibitory effects on eIF4A, we sought to determine whether this mechanism participates in the control of IFN-inducible gene (ISG) - protein products that mediate generation of IFNα - responses. For this purpose, serum starved KT1 cells

were treated with IFNα in the presence or absence of the proteasomal inhibitor MG132. As expected, treatment with MG132 stabilized PDCD4 and reversed IFNα-inducible degradation of the protein (Fig. 6A). This stabilization of PDCD4 protein correlated with suppression of induction of gene-products with important roles in the generation of the biological effects of IFNs, including ISG15 (58), $p21^{WAF1/CIP1}$ (17), and SLFN5 (18) (Fig. 6A). To determine whether RSK1-mediated phosphorylation of PDCD4 is important for these responses, we assessed the effects of RSK inhibitor SL0101-1 on IFN-inducible expression of ISG15, $p21^{WAF1/CIP1}$, and SLFN5. IFNα-dependent induction of expression of ISG15 (Fig. 6B), $p21^{WAF1/CIP1}$ (Fig.6C) and SLFN5 (Fig. 6D) was partially reversed by pre-treatment of cells with SL0101-1. This defective ISG15, $p21^{WAF1/CIP1}$ and SLFN5 protein expression in cells pretreated with SL0101-1 was not associated with decreased IFN-dependent mRNA induction/transcription of the *Isg15* (Fig. 6E), *p21*$^{WAF1/CIP1}$ (Fig.6F) or *Slfn5* (Fig. 6G) genes, suggesting that this may be the result of defective mRNA translation/protein expression. In experiments in which RSK1 expression was knocked down using siRNAs, there was also defective IFN-dependent ISG15 protein expression (Fig. 6H). Altogether, these studies suggest that the IFNα-induced RSK1 kinase activity is required for phosphorylation and subsequent degradation of PDCD4, possibly by promoting initiation of cap-dependent mRNA translation of ISGs.

We also performed studies in which a PDCD4 wild type or mutant for the RSK1 phosphorylation site (PDCD4-S67/71A) was overexpressed in KT1 cells and IFNα-dependent ISG protein expression was examined. As shown in Fig. 7A, induction of ISG15, $p21^{WAF1/CIP1}$, and SLFN5 protein was defective in cells in which PDCD4-S67/71A was expressed, establishing potent negative regulatory effects of

377 unphosphorylated PDCD4 on ISG-expression. Thus, IFNα-dependent, RSK1-mediated,
378 phosphorylation of PDCD4 on Ser67 is essential for proteasomal degradation of the
379 protein and this regulatory mechanism is critical for expression of ISG proteins that
380 mediate the biological effects of IFNs. Notably, in experiments in which PDCD4 was
381 knocked down by specific siRNAs, IFN-dependent expression of several key ISG
382 proteins, including ISG15 (Fig. 7B), $p21^{WAF1/CIP1}$ (Fig. 7C), as well as SLFN5 (Fig. 7C)
383 was further enhanced. In addition, an increase in the basal levels of expression of SLFN5
384 and $p21^{WAF1/CIP1}$ was noticeable (Fig. 7C).

385 In subsequent studies, we sought to directly determine whether mRNA translation
386 for ISG15, $p21^{WAF1/CIP1}$ and SLFN5 genes is enhanced in cells in which PDCD4 is
387 knocked down. For this purpose, polysomal mRNA from KT1 cells transduced with
388 control shRNA, or shRNA specifically targeting human PDCD4, was isolated and Pdcd4
389 mRNA expression prior to and after IFN-treatment was assessed in polysomal fractions.
390 The polysomal profiles from KT1 cells transduced with control shRNA or with shRNA
391 targeting the PDCD4, before and after IFNα treatment, are shown in Fig. 8A. There was
392 a significant increase of *Isg15* (Fig. 8B) and *Slfn5* (Fig.8C) mRNA in polysomes isolated
393 from cells that were IFNα treated and transduced with shRNA targeted against PDCD4,
394 as compared to cells that were IFNα treated and transduced with control shRNA (Fig. 8 B
395 and C), establishing regulatory effects of Pdcd4 on ISG mRNA translation.

396 We have previously shown that RSK1 plays an essential role in the generation of the
397 suppressive effects of IFNα on primitive leukemic precursors (CFU-L), and have
398 identified eIF4B as a downstream phosphorylation target and mediator of these effects
399 (23). We examined whether phosphorylation of PDCD4 by activated RSK1 plays a role

400 in the generation of the anti-leukemic effects of IFNα. For this purpose, the effects of
401 PDCD4 knockdown or expression of mutant PDCD4 (S67/71A) on the generation of the
402 effects of IFNα on primitive KT1-derived leukemic progenitors were assessed by
403 clonogenic assays in methylcellulose. Suppression of CFU-L growth after IFNα
404 treatment was further enhanced in PDCD4 knockdown cells, as compared to control
405 siRNA transfected cells (Fig. 9A). On the other hand, expression of the PDCD4
406 (S67/71A) mutant significantly reversed the inhibitory effects of IFNα on CFU-L colony
407 formation as compared with control empty vector, or ectopic expression of WT PDCD4
408 (Fig. 9B). In other studies, we assessed the potential regulatory roles of RSK1 and
409 PDCD4 on normal bone marrow-derived (CFU-GM) progenitor colony formation. As
410 shown in Fig. 10A, siRNA-mediated PDCD4 knockdown resulted in enhancement of the
411 suppressive effects of IFNα on normal CFU-GM colonies, while RSK1 knockdown had
412 opposing effects and partially reversed the inhibitory effects of IFNα (Fig. 10A). These
413 findings suggest that RSK1-mediated phosphorylation and subsequent degradation of
414 PDCD4 relieves the inhibitory effects of the protein on the generation of IFN-biological
415 responses. Consistent with this, expression of the PDCD4 S67/71 mutant in CD34+
416 cells, resulted in reversal of the effects of IFNα on normal CFU-GM (Fig. 10B),
417 underscoring the functional relevance of IFN-dependent PDCD4 phosphorylation.
418
419
420
421

Discussion

IFNs are pleiotropic cytokines with important biological properties that were originally defined as key elements of the host defense against viral infections (35, 47). Beyond eliciting antiviral responses, IFNs exhibit important immuno-modulatory and antineoplastic activities and play key roles in the immune surveillance against malignancies (35, 47). IFNs generate their biological effects by engaging JAK-STAT signaling pathways, leading to the transcriptional activation of ISGs and the expression of their protein products, which promote diverse IFN-responses (29, 30, 39, 43, 47). Beyond activation of classical JAK-STAT pathways by IFNs, there has been emerging evidence in recent years for the existence of several additional "non-classical" IFNR-activated cellular cascades which complement the function of JAK-STAT pathways and optimize expression of ISGs (40). Engagement of the p38 MAPK pathway is required for optimal ISG transcription and induction of IFN-responses (50), while members of the PKC-family of proteins play key roles in complementing transcriptional activation of ISGs via modulating STAT serine phosphorylation and and/or acting as regulators of other IFN-induced cellular responses (42, 51). We previously demonstrated that the PI3'-kinase/Akt/mTOR/S6K pathway activated by IFNs is essential for IFN-dependent mRNA translation of key ISGs (19-23). Importantly, we recently provided evidence for co-ordination between the mTOR pathway and MAPK regulated cascades in ISG mRNA translation, as shown by the requirement for IFN-induced, MEK/ERK-dependent MNK kinases in eIF4E phosphorylation and mRNA translation of ISGs (15, 16). Such co-ordination of MAPK and mTOR pathways in the regulation of mRNA translation of IFN-induced genes is also evident by the cell type-specific involvement in the process of the

kinase RSK1, an effector of the MEK/ERK cascade (23). In previous work we demonstrated that phosphorylation/activation of eIF4B in the IFN-system occurs either by the activity of the S6K downstream of mTOR or via RSK1, an effector of the MEK/ERK cascade (23). In addition, in the Type III (IFNλ) system, RSK1 appears to be the primary kinase that controls 4E-BP1 phosphorylation in HT-29 colorectal cells (22).

PDCD4, a tumor suppressor protein for which the human gene is located on chromosome band 10q24 (46), has important regulatory functions in mammalian cells (3, 14, 24, 25, 33, 54, 56). This protein interacts with eIF4A (25, 48, 53, 55) and negatively controls the helicase activity of eIF4A and cap-dependent translation (37, 48, 55). Notably, beyond free eIF4A, PDCD4 inhibits the function of eIF4F-bound eIF4A (24, 53, 55), providing a mechanism by which it may be acting as a suppressor of mRNA translation (48, 55). There is also evidence that PDCD4 binds RNA and interacts with eIF4G *in vitro* (2, 48, 55). PDCD4 expression is regulated by multiple mechanisms (25). Previous studies have shown that increase in miR-21 (microRNA-21) results in PDCD4 down-regulation (7). Another mechanism for regulation of the PDCD4 involves its phosphorylation by Akt and S6K1, leading to proteosomal degradation (9, 34). This mechanism may also apply in the context of constitutive mTOR/S6K activation, as seen in response to transformation of cells by oncogene proteins such as BCR-ABL (4).

As IFNRs are known to activate the mTOR/S6K pathway, we sought to determine the effects IFN-treatment on PDCD4 phosphorylation. Our data demonstrate that treatment of cells with IFNα results in phosphorylation of PDCD4 on serine 67. Importantly, this IFN-dependent phosphorylation of PDCD4 results in an association of

468 the protein with the ubiquitin ligase $SCF^{\beta TrCP}$ (9, 10), ultimately leading to its
469 degradation. IFN-dependent phosphorylation of PDCD4 occurred in an S6K-dependent
470 manner in MEF cells, but it was found to be MEK/ERK-dependent and RSK1-mediated
471 in the malignant hematopoietic cell lines KT1 and U266. Thus, as in the case of eIF4B
472 (23), RSK1 appears to be the dominant kinase that regulates phosphorylation of PDCD4
473 in hematopoietic cells. Remarkably, our data demonstrate that PDCD4 exhibits negative
474 regulatory effects on the eIF4F complex, and on the expression of ISGs with important
475 functions in the generation of IFN-responses, including ISG15, $p21^{Waf1/Cip1}$ and SLFN5
476 (17, 18, 58). Such PDCD4-mediated effects on the expression of these ISG products
477 appears to reflect inhibitory effects of PDCD4 on cap-dependent mRNA translation,
478 which, based on previous work, is required for ISG expression. In studies to define the
479 functional relevance of PDCD4 in the generation of the biological effects of IFNα, we
480 found that siRNA-mediated knockdown of PDCD4 enhanced the suppressive effects of
481 IFNα on primitive hematopoietic precursors from normal marrows and leukemic CFU-L
482 progenitors. On the other hand, ectopic expression of the PDCD4 S67/71A mutant
483 reversed the suppressive effects of IFNα on normal myeloid and leukemic progenitor
484 colony formation, suggesting that PDCD4 inhibits IFN-responses, likely via suppressive
485 effects on ISG mRNA translation.

486 There is extensive previous work demonstrating that PDCD4 is a tumor
487 suppressor (3, 12, 53) and that its expression is decreased in several malignancies (11, 12,
488 14, 31, 33, 44, 53). PDCD4 has also been shown to regulate cell-cycle progression in a
489 cell type specific manner and to inhibit cell proliferation (13). The finding that this
490 protein antagonizes and negatively controls generation of the growth suppressive effects

of IFNα is at first glance surprising and somewhat unexpected. However, it should be noted that there is previous evidence for some opposing cellular regulatory roles of PDCD4, depending on the cell type and context. For instance, PDCD4 increases $p21^{Waf1/Cip1}$ and suppresses CDK1 and CDC2 expression in neuroendocrine cells (13), while in HCT116 colon adenocarcinoma cells appears to negatively control $p21^{Waf1/Cip1}$ levels (1). The findings of the current study indicate that in the case of Type IFNs, PDCD4 negatively controls mRNA translation/protein expression of several IFN-induced genes with antiproliferative properties, including $p21^{Waf1/Cip1}$, SLFN5 and ISG15. Importantly, such a role for PDCD4 in the IFN-system is consistent with the positive regulatory effects of mTOR- and RSK-mediated signals in the mRNA translation/expression of ISG products (19-23). In future studies it will be important to define the functional role of PDCD4 in the signaling pathways of other cytokines with antineoplastic properties, as this may lead to the identification of unexpected novel targets and new approaches to block malignant cell growth with potentially important therapeutic implications.

Acknowledgements

This work was supported by NIH grants CA77816, CA15566, and CA161796; and a Merit Review grant from the Department of Veterans Affairs. We thank Dr. Sara Kozma (University of Cincinnati) for providing MEF cells from S6K knockout mice.

References

1. **Bitomsky, N., N. Wethkamp, R.Marikkannu, and K.H. Klempnauer.** 2008. siRNA-mediated knockdown of Pdcd4 expression causes up regulation of p21$^{Waf1/Cip1}$ expression. Oncogene **27**:4820–4829.
2. **Bohm, M., K. Sawicka, J.P. Siebrasse, A. Brehmer-Fastnacht, R. Peters, and K.H. Klempnauer.** 2003. The transformation suppressor protein Pdcd4 shuttles between nucleus and cytoplasm and binds RNA. Oncogene **22:** 4905–4910.
3. **Cmarik, J.L., H. Min, G. Hegamyer, S. Zhan, M. Kulesz-Martin, H. Yoshinaga, S. Matsuhashi, and N.H. Colburn.** 1999. Differentially expressed protein Pdcd4 inhibits tumor promoter-induced neoplastic transformation. Proc. Natl. Acad. Sci. U.S.A. **96**:14037–14042.
4. **Carayol, N., E. Katsoulidis, A. Sassano, J. K. Altman, B. J. Druker, and L.C. Platanias.** 2008. Suppression of programmed cell death 4 (PDCD4) protein expression by BCR-ABL-regulated engagement of the mTOR/p70 S6 kinase pathway. J. Biol. Chem. **283**:8601-8610.
5. **Critchley-Thorne, R. J., D.L. Simons, N. Yan, A.K. Miyahira, F.M. Dirbas, D.L. Johnson, S.M. Swetter, R.W. Carlson, G.A. Fisher, A. Koong, S. Holmes, and P.P. Lee.** 2009. Impaired interferon signaling is a common immune defect in human cancer. Proc. Natl. Acad. Sci. U. S. A. **106:**9010-9015.
6. **Darnell, J. E., Jr. I. M. Kerr, and G. R. Stark.** 1994. Jak-STAT pathways and transcriptional activation in response to IFNs and other extracellular signaling proteins. Science **264:**1415-1420.

7. **Davis, B. N., A. C. Hilyard, G. Lagna, A. Hata.** 2008. SMAD proteins control DROSHA-mediated microRNA maturation. Nature **454**:56-61.

8. **Donnelly, R.P., and S.V. Kotenko**. 2010. Interferon-lambda: a new addition to an old family. J. Interferon Cytokine Res. **30:**555-564.

9. **Dorrello, N. V., A. Peschiaroli, D. Guardavaccaro, N. H. Colburn, N. E. Sherman, and M. Pagano.** 2006. S6K1- and ßTRCP-mediated degradation of PDCD4 promotes protein translation and cell growth. Science **314:**467-471.

10. **Frescas, D., and M. Pagano**. 2008. Deregulated proteolysis by the F-box proteins SKP2 and beta-TrCP: tipping the scales of cancer. Nat. Rev. Cancer **8:**438-449.

11. **Gao, F., X. Wang, F. Zhu, Q. Wang, X. Zhang, C. Guo, C. Zhou, C. Ma, W. Sun, Y. Zhang, Y.H. Chen, and L. Zhang.** 2008. PDCD4 gene silencing in gliomas is associated with 5′CpG island methylation and unfavorable prognosis. J. Cell. Mol, Med., doi:10.1111/j.1582-4934.2008.00497.x

12. **Göke, R., C. Gregel, A. Göke, R. Arnold, H. Schmidt, and B. Lankat-Buttgereit.** 2004. Programmed cell death protein 4 (PDCD4) acts as a tumor suppressor in neuroendocrine tumor cells. Ann. N.Y. Acad. Sci. **1014**:220-221.

13. **Göke, R., P. Barth, A. Schmidt, B. Samans, and B. Lankat-Buttgereit.** 2004. Programmed cell death protein 4 suppresses CDK1/cdc2 via induction of p21(Waf1/Cip1). Am. J. Physiol. Cell Physiol. **28**7:C1541–C1546.

14. **Hilliard, A., B. Hilliard, S.J Zheng, H. Sun, T. Miwa, W. Song, R. Goke, and Y.H. Chen.** 2006. Translational regulation of autoimmune inflammation and lymphoma genesis by programmed cell death 4. J. Immunol. **177**:8095–8102.

15. **Joshi, S., S. Kaur, A.J. Redig, K. Goldsborough, K. David, T. Ueda, R. Watanabe-Fukunaga, D.P. Baker, E.N. Fish, R. Fukunaga, and L.C. Platanias.** 2009. Type I interferon (IFN)-dependent activation of Mnk1 and its role in the generation of growth inhibitory responses. Proc. Natl. Acad. Sci. U. S. A. **106:**12097-12102.

16. **Joshi, S.**, **B. Sharma, S. Kaur, B. Majchrzak, T. Ueda, R. Fukunaga, A. K. Verma, E. N. Fish, and L. C. Platanias**. 2011. Essential role for Mnk kinases in Type II interferon (IFNγ) signaling and its suppressive effects on normal hematopoiesis. J. Biol. Chem. **286:**6017-6026.

17. **Katayama, T., K. Nakanishi, H. Nishihara, N. Kamiyama, T. Nakagawa, T. Kamiyama, K. Iseki, S. Tanaka, and S. Todo.** 2007. Type I interferon prolongs cell cycle progression via p21WAF1/CIP1 induction in human colon cancer cells. Int. J. Oncol. **31**:613-620.

18. **Katsoulidis, E., E. Mavrommatis, J. Woodard, M. A. Shields, A. Sassano, N. Carayol, K. T. Sawicki, H. G. Munshi, and L. C. Platanias**. 2010. Role of interferon {alpha} (IFN{alpha})-inducible Schlafen-5 in regulation of anchorage-independent growth and invasion of malignant melanoma cells. J. Biol. Chem. **285:**40333-40341.

19. **Kaur, S., L. Lal, A. Sassano, B. Majchrzak-Kita, M. Srikanth, D.P. Baker, E. Petroulakis, N. Hay, N. Sonenberg, E.N. Fish, and L.C. Platanias.** 2007. Regulatory effects of mammalian target of rapamycin-activated pathways in type I and II interferon signaling. J. Biol. Chem. **282:**1757-1768.

599 **20. Kaur, S., A. Sassano, B. Dolniak, S. Joshi, B. Majchrzak-Kita, D.P. Baker,**
600 **N. Hay, E.N. Fish, and L.C. Platanias**. 2008. Role of the Akt pathway in mRNA
601 translation of interferon-stimulated genes. Proc. Natl. Acad. Sci. U. S. A. **105**:
602 4808-4813.
603 **21. Kaur, S., A. Sassano, A.M. Joseph, B. Majchrzak-Kita, E.A. Eklund,**
604 **A.Verma, S.M. Brachmann, E.N. Fish, and L.C. Platanias.** 2008. Dual
605 regulatory roles of phosphatidylinositol 3-kinase in IFN signaling. J. Immunol.
606 **181**:7316-7323.
607 **22. Kroczynska, B., S. Joshi, E. A. Eklund, A. Verma, S. V. Kotenko, E. N. Fish,**
608 **and L. C. Platanias.** 2011. Regulatory effects of ribosomal S6 kinase 1 (RSK1)
609 in IFNλ signaling. J. Biol. Chem. **286:**1147-1156.
610 **23. Kroczynska, B., S. Kaur, E. Katsoulidis, B. Majchrzak-Kita, A. Sassano, S.**
611 **C. Kozma, E.N. Fish, and L.C. Platanias.** 2009. Interferon-dependent enga-
612 gement of eukaryotic initiation factor 4B via S6 kinase (S6K)- and ribosomal
613 protein S6K-mediated signals. Mol. Cell Biol. **29**:2865-2875.
614 **24. Lankat-Buttgereit, B., and R. Goke.** 2005. Programmed cell death 4 (Pdcd4) -
615 a potential target for new approaches in cancer therapy. Curr. Topics Peptide
616 Prot. Res. **7:**63–66.
617 **25. Lankat-Buttgereit, B., and R. Göke.** 2009. The tumor suppressor Pdcd4: recent
618 advances in the elucidation of function and regulation. Biol. Cell.**101**:309-317.
619 **26. Leighton, I.A., K.N. Dalby, F.B. Caudwell, P.T. Cohen, P. Cohen**. 1995.
620 Comparison of the specificities of p70 S6 kinase and MAPKAP kinase-1
621 identifies a relatively specific substrate for p70 S6 kinase: the N-terminal kinase

domain of MAPKAP kinase-1 is essential for peptide phosphorylation. FEBS Lett. **375**:289-293

27. **Lekmine, F., A. Sassano, S. Uddin, J. Smith, B. Majchrzak, S. M. Brachmann, N. Hay, E. N. Fish, and L. C. Platanias.** 2004. Interferon-gamma engages the p70 S6 kinase to regulate phosphorylation of the 40S S6 ribosomal protein. Exp. Cell Res. **295:**173-182.

28. **Lekmine, F., S. Uddin, A. Sassano, S. Parmar, S. M. Brachmann, B. Majchrzak, N. Sonenberg, N. Hay, E. N. Fish, and L. C. Platanias.** 2003. Activation of the p70 S6 kinase and phosphorylation of the 4E-BP1 repressor of mRNA translation by type I interferons. J. Biol. Chem. **278:**27772-27780.

29. **Levy, D.E.** 1997. The house that Jak/Stat built. Cytokine Growth Factor Rev. **8:**81-90.

30. **Levy, D.E., and J.E. Darnell Jr.** 2002. Stats: transcriptional control and biological impact. Nat. Rev. Mol. Cell Biol. **3:**651-662.

31. **Matsuhashi, S., Y. Narisawa, I. Ozaki, and T. Mizuta.** 2007. Expression patterns of programmed cell death 4 protein in normal human skin and some representative skin lesions. Exp. Dermatol. **16**:179–184.

32. **Moritz A., Y. Li, A. Guo, J. Villén, Y. Wang, J. MacNeill, J. Kornhauser, K. Sprott, J. Zhou, A. Possemato, J.M. Ren, P. Hornbeck, L.C. Cantley, S.P. Gygi, J. Rush, M.J. Comb.** 2010. Akt-RSK-S6 kinase signaling networks activated by oncogenic receptor tyrosine kinases. Sci Signal. **3** (136):ra64.

33. **Mudduluru, G., F. Medved, R. Grobholz, C. Jost, A. Gruber, J.H. Leupold, S. Post, A. Jansen, N.H. Colburn, and H. Allgayer.** 2007. Loss of programmed

cell death 4 expression marks adenoma-carcinoma transition, correlates inversely with phosphorylated protein kinase B, and is an independent prognostic factor in resected colorectal cancer. Cancer **110**:1697–1707.

34. Palamarchuk, A., A. Efanov, V. Maximov, R.I. Aqeilan, C.M. Croce, and Y. Pekarsky. 2005. Akt phosphorylates and regulates Pdcd4 tumor suppressor protein. Cancer Res. **65:**11282-11286.

35. Parmar, S., and L.C. Platanias. 2003. Interferons: mechanisms of action and clinical applications. Curr. Opin. Oncol. **15**:431-439.

36. Parmar, S., J. Smith, A. Sassano, S. Uddin, E. Katsoulidis, B. Majchrzak, S. Kambhampati, E.A. Eklund, M.S. Tallman, E.N. Fish, and L.C. Platanias. 2005. Differential regulation of the p70 S6 kinase pathway by interferon alpha (IFNalpha) and imatinib mesylate (STI571) in chronic myelogenous leukemia cells. Blood. **106**:2436-2443.

37. Parsyan, A., Y. Svitkin , D. Shahbazian , C. Gkogkas , P. Lasko, W. C. Merrick , N. Sonenberg . 2011. mRNA helicases: the tacticians of translational control. Nat Rev Mol Cell Biol.**12**:235-245.

38. Pende, M., S. H. Um, V. Mieulet, M. Sticker, V. L. Goss, J. Mestan, M. Mueller, S. Fumagalli, S. C. Kozma, and G. Thomas. 2004. S6K1$^{-/-}$/S6K2$^{-/-}$ mice exhibit perinatal lethality and rapamycin-sensitive 5'-terminal oligopyrimidine mRNA translation and reveal a mitogen-activated protein kinase-dependent S6 kinase pathway. Mol. Cell. Biol. **24:**3112-3124.

39. Platanias, L.C. 2005. Mechanisms of type-I- and type-II-interferon-mediated signaling. Nat. Rev. Immunol. **5**:375-386.

668 **40. Platanias, L.C.** 2005. Introduction: interferon signals: what is classical and
669 what is nonclassical? J. Interferon Cytokine Res. **25**:732.
670 **41. Powers, M.A., M.M. Fay, R.E. Factor, A.L. Welm, and K.S. Ullman**. 2011.
671 Protein Arginine Methyltransferase 5 Accelerates Tumor Growth by Arginine
672 Methylation of the Tumor Suppressor Programmed Cell Death 4. Cancer Res.
673 **71**:5579-5587.
674 **42. Redig, A.J., A. Sassano, B. Majchrzak-Kita, E. Katsoulidis, H. Liu, J.K.**
675 **Altman, E.N. Fish, A. Wickrema, and L.C. Platanias.** 2009. Activation of
676 protein kinase C eta (PKCη) by type I interferons. J. Biol. Chem. **284:**10301-
677 10314.
678 **43. Schindler, C**., **D.E. Levy, and T. Decker**. 2007. JAK-STAT signaling: from
679 interferons to cytokines. J. Biol. Chem. **282:**20059-20063.
680 **44. Schmid, T., A.P. Jansen, A.R. Baker, G. Hegamyer, J.P. Hagan, and N.H.**
681 **Colburn.** 2008. Translation inhibitor Pdcd4 is targeted for degradation during
682 tumor promotion. Cancer Res. **68:**1254–1260.
683 **45. Sharma, B., J. K. Altman, D. J. Goussetis, A. K. Verma, and L. C. Platanias.**
684 2011. Protein kinase R (PKR) as mediator of the effects of IFN-gamma and
685 TNF-alpha on normal and dysplastic hematopoiesis. J. Biol. Chem. **286**:27506-
686 27514.
687 **46. Soejima, H., O. Miyoshi, H. Yoshinaga, Z. Masaki, I. Ozaki, S. Kajiwara, N.**
688 **Niikawa, S. Matsuhashi, and T. Mukai.** 1999. Assignment of the programmed
689 cell death 4 gene (PDCD4) to human chromosome band 10q24 by *in situ*
690 hybridization. Cytogenet. Cell Genet. **87:**113–114.

691 **47. Stark, G. R., I. M. Kerr, B. R. Williams, R. H. Silverman, and R. D.**
692 **Schreiber.** 1998. How cells respond to interferons. Annu. Rev. Biochem.
693 **67:**227-264.
694 **48. Suzuki, C., R. G. Garces , K. A. Edmonds , S. Hiller , S. G. Hyberts , A.**
695 **Marintchev , G. Wagner .** 2008. PDCD4 inhibits translation initiation by
696 binding to eIF4A using both its MA3 domains. Proc Natl Acad Sci U S A. **105**:
697 3274-3279.
698 **49. Tai, A.W., and R.T. Chung**. 2009. Treatment failure in hepatitis C: mechanisms
699 of non-response. J. Hepatol. **50:**412-420.
700 **50. Uddin, S., F. Lekmine, N. Sharma, B. Majchrzak, I. Mayer, P.R. Young,**
701 **G.M. Bokoch, E.N. Fish, and L.C. Platanias.** 2000. The Rac1/p38 mitogen-
702 activated protein kinase pathway is required for interferon alpha-dependent
703 transcriptional activation but not serine phosphorylation of Stat proteins. J. Biol.
704 Chem. **275:**27634-27640.
705 **51. Uddin, S., A. Sassano, D.K. Deb, A. Verma, B. Majchrzak, A. Rahman, A.B.**
706 **Malik, E.N. Fish, and L.C. Platanias.** 2002. Protein kinase C-delta (PKC-
707 delta) is activated by type I interferons and mediates phosphorylation of Stat1 on
708 serine 727. J. Biol. Chem. **277**:14408-14416.
709 **52. Wang A., J. Rud, C.M. Olson Jr, J Anguita, B.A. Osborne . 2009.**
710 Phosphorylation of Nur77 by the MEK-ERK-RSK cascade induces
711 mitochondrial translocation and apoptosis in T cells. J Immunol. **183**:3268-3277.
712 **53. Waters, L.C., S.L. Strong, E. Ferlemann, O. Oka, F.W. Muskett, V.**
713 **Veverka, S. Banerjee, T. Schmedt, A.J. Henry, K.H. Klempnauer, and M.D.**

Carr. 2011. Structure of the tandem MA-3 region of Pdcd4 protein and characterization of its interactions with eIF4A and eIF4G: molecular mechanisms of a tumor suppressor. J. Biol. Chem. **286:**17270-17280.

54. Wen, Y.H., X. Shi, L. Chiriboga, S.Matsahashi, H. Yee, and O. Afonja. 2007. Alterations in the expression of PDCD4 in ductal carcinoma of the breast. Oncol. Rep. **18**:1387–1393.

55. Yang, H. S., A. P. Jansen, A. A. Komar, X. Zheng, W. C. Merrick, S. Costes, S. J. Lockett, N. Sonenberg, and N. H. Colburn. 2003. The transformation suppressor Pdcd4 is a novel eukaryotic translation initiation factor 4A binding protein that inhibits translation. Mol. Cell Biol. **23**:26-37.

56. Yang, H.S., A.P. Jansen, R. Nair, K. Shibahara, A.K. Verma, J.L. Cmarik, and N.H. Colburn. 2001. A novel transformation suppressor, Pdcd4, inhibits AP-1 transactivation but not NF-κkappaB or ODC transactivation. Oncogene **20**:669–676.

57. Yang, Y.F., W. Zhao, Y.D. Zhong, H.M. Xia, L. Shen, and N. Zhang. 2009. Interferon therapy in chronic hepatitis B reduces progression to cirrhosis and hepatocellular carcinoma: a meta-analysis. J. Viral Hepat. **16**:265-271.

58. Zhang, D., and D.E. Zhang. 2011. Interferon-stimulated gene 15 and the protein ISGylation system. J. Interferon Cytokine Res. **31**:119-130.

59. Zivadinov, R., A.T. Reder, M. Filippi, A. Minagar, O. Stüve, H. Lassmann, M.K. Racke, M.G. Dwyer, E.M. Frohman, and O. Khan. 2008. Mechanisms of action of disease-modifying agents and brain volume changes in multiple sclerosis. Neurology **71:**136-144.

Figure Legends

Figure 1: Effects of IFNα on phosphorylation and degradation of PDCD4 in MEFs. (A) *(Upper panel)* Serum starved S6k1+/+S6k2+/+ (WT) and S6k1-/-S6k2-/- MEFs, were treated with IFNα for the indicated times. Total cell lysates were resolved by SDS-PAGE and immunoblotted with antibodies against the phosphorylated form of PDCD4 on Ser67 or against PDCD4 as indicated. *(Lower panel)* Signals were quantified by densitometry and used to calculate the intensity of phosphorylated PDCD4 relative to that of total PDCD4. Data are expressed as ratios of phospho-PDCD4 to PDCD4 for each experimental condition and represent means ± SE of the results of three experiments, including the one shown in the upper panel. (B) Serum starved wild-type (WT) MEFs were pre-treated for 60 minutes with rapamycin or U0126 and were subsequently treated with IFNα for the indicated times. Cell lysates were resolved by SDS-PAGE and immunoblotted with anti-phospho-Ser67-PDCD4, anti-PDCD4, anti-phospho-Thr202/Tyr204-ERK1/2 or anti-ERK1/2 antibodies, as indicated. (C) Serum starved S6k1+/+S6k2+/+ (WT) or S6k1-/-S6k2-/- MEFs were incubated with IFNα for 6 hours, as indicated. Total cell lysates were resolved by SDS-PAGE and immunoblotted with antibodies against PDCD4 or against GAPDH, as indicated. (D) Serum starved WT MEFs were pre-treated for 60 min with rapamycin or U0126 and were subsequently treated with IFNα in the continuous presence or absence of rapamycin or U0126 for 6 hours as indicated. The cells were lysed, and total cell lysates were resolved by SDS-PAGE and immunoblotted with antibodies against PDCD4 or against GAPDH, as indicated. (E) Serum starved S6k1+/+S6k2+/+ MEFs were treated with IFNα for the indicated times in presence or absence of the proteasome inhibitor MG132. Total cell

lysates were resolved by SDS-PAGE and immunoblotted with anti-PDCD4 or anti-GAPDH antibodies, as indicated.

Figure 2: IFN-dependent regulation of PDCD4 phosphorylation and protein expression in KT1 hematopoietic cells. (A) Serum starved KT1 cells were pretreated for 60 min with rapamycin or the MEK inhibitor U0126 and were subsequently treated with IFNα in the continuous presence or absence of rapamycin or U0126, for the indicated times. Cell lysates were resolved by SDS-PAGE and immunoblotted with anti-phospho-Ser67-PDCD4, anti-PDCD4, anti-phospho-Thr202/Tyr204-ERK1/2, anti-ERK1/2, anti-phospho-S6K, and S6K, antibodies as indicated. (B) Similar experiment as in (A), except that cells were pre-treated for 60 min with rapamycin or for 180 min with SL0101-1. Total cell lysates were resolved by SDS-PAGE and immunoblotted with anti-phospho-Ser67-PDCD4, anti-phospho-Ser221-RSK1, anti-RSK1, anti-S6K, as indicated. Equal cell lysates from the same experiment were analyzed separately by SDS-PAGE and immunoblotted with anti-PDCD4, anti-phospho-Thr421/Ser424-S6K, anti-phospho-Ser240/244-S6rp, and anti-S6rp. (C) *(Upper panel)* Similar experiment as in (B), except that the cells were treated for 6 hours as indicated. Protein lysates were analyzed by immunoblotting with antibodies against PDCD4 or against GAPDH. *(Lower panel)* Signals were quantified by densitometry and used to calculate the intensity of expression of PDCD4 relative to that of GAPDH. Data are expressed as ratios of PDCD4 to GAPDH for each experimental condition and represent means $\pm$ SE of the results of three experiments, including the experiment shown in the upper panel. (D) Serum starved U266 cells were pre-treated for 60 min with rapamycin or 3 hours with SL0101-1 and

783 were subsequently treated with IFNα in the continuous presence or absence of rapamycin
784 or SL0101-1, as indicated. Cell lysates were resolved by SDS-PAGE and immunoblotted
785 with anti-phospho-Ser67-PDCD4, anti-PDCD4, anti-phospho-Ser240/244-S6rp, or anti
786 S6rp, as indicated. (E) Serum starved U266 cells were pretreated for 60 min with
787 rapamycin or 3 hours with SL0101-1, as indicated and were subsequently treated with
788 IFNα in the continuous presence or absence of the indicated inhibitors for 6 hours. Cell
789 lysates were resolved by SDS-PAGE and immunoblotted with anti-PDCD4 or anti-
790 GAPDH antibodies, as indicated.
791
792 **Figure 3: RSK1 activity mediates IFNα-dependent PDCD4 phosphorylation in**
793 **hematopoietic cells**. (A) KT1 cells were transfected with either control siRNA or
794 siRNAs specifically targeting RSK1, and after serum starvation were treated with IFNα,
795 as indicated. Total cell lysates were resolved by SDS-PAGE and immunoblotted with
796 anti-RSK1, anti-phospho-Ser67-PDCD4, anti-PDCD4, or anti-GAPDH antibodies, as
797 indicated. (B) Serum-starved KT1 cells were pretreated with SL0101-1 for 3 hours and
798 then treated with IFNα for the indicated times. The cells were lysed and equal amounts
799 of protein were immunoprecipitated with an anti-RSK1 antibody. In *vitro* kinase assays
800 to detect RSK1 activity were subsequently carried out on the immunoprecipitates, using
801 PDCD4 protein as an exogenous substrate.
802
803 **Figure 4: IFNα-inducible Ser67 PDCD4 phosphorylation results in its interaction**
804 **with βTRCP.** (A) Serum starved KT1 cells were pre-treated for 3 hours with SL0101-1
805 and were left untreated or treated with IFNα, in the continuous presence or absence of

SL0101-1, as indicated. Equal amounts of cell lysates were immunoprecipitated with an anti-βTRCP antibody, or control non-immune rabbit IgG (RIgG). Immune complexes were resolved by SDS-PAGE for analysis of PDCD4, and βTRCP, as indicated. (B) KT1 cells were transfected with either control siRNA or RSK1 siRNA, and after serum starvation were either left untreated or treated with IFNα for 30 min as indicated. Equal amounts of cell lysates were immunoprecipitated with an anti-βTRCP antibody, or control RIgG. Immune complexes were resolved by SDS-PAGE for analysis of PDCD4, and βTRCP, as indicated. (C) Similar experiment as in (A), except that, equal amounts of cell lysates were immunoprecipitated with an anti-eIF4A antibody, or control non-immune goat IgG (GIgG). Immune complexes were resolved by SDS-PAGE for analysis of PDCD4, eIF4G, and eIF4A, as indicated. (D) Similar experiment as in (B), except that, equal amounts of cell lysates were immunoprecipitated with an anti-eIF4A antibody, or control GIgG. Immune complexes were resolved by SDS-PAGE for analysis of PDCD4, eIF4G, and eIF4A, as indicated. (E) Lysates for the different experimental conditions from the experiment shown in D were resolved by SDS-PAGE and immunoblotted by anti-RSK1 or anti-GAPDH antibodies to establish RSK1 knockdown in cells transfected with siRNA against RSK1.

Figure 5: Regulation of Type I IFN-inducible binding of eIF4G and eIF4A to the 7-methylguanosine cap complex by PDCD4. (A) Serum starved KT1 cells were pre-treated for 60 min with rapamycin or for 3 hours with SL-0101-1 and were subsequently treated with IFNα in the continuous presence or absence of SL-0101-1, for the indicated times. Total cell lysates were bound to the cap analog m^7GTP conjugated to beads and

bound proteins were resolved by SDS-PAGE and immunoblotted with the indicated antibodies. The lysates used were the same from the experiment shown in Fig. 2, panel C. **(**B**)** KT1 cells were transfected with either control siRNA or RSK1 siRNA, and after serum starvation were either left untreated or treated with IFNα for 6 hours as indicated. Total cell lysates were resolved by SDS-PAGE and immunoblotted with the indicated antibodies. (C) Cell lysates from the experiment shown in panel B were bound to the cap analog m^7GTP conjugated to beads, and after extensive washing bound proteins were resolved by SDS-PAGE and immunoblotted with the indicated antibodies. (D) KT1 cells were transfected with either control siRNA or PDCD4 siRNA, and after serum starvation were either left untreated or treated with IFNα for 6 hours as indicated. Total cell lysates were resolved by SDS-PAGE and immunoblotted with the indicated antibodies. (E) Cell lysates from the experiment shown in panel D were bound to the cap analog m^7GTP conjugated to beads, and after extensive washing bound proteins were resolved by SDS-PAGE and immunoblotted with the indicated antibodies. For the anti-eIF4G blot, two different exposures of the same blot (a shorter and a longer exposure) are shown in the upper 2 panels. (F) *(Upper panel)* KT1 cells were transfected with HA-tagged PDCD4 wt or S67/71A PDCD4 mutant or empty vector as indicated, serum starved and treated with IFNα as indicated. Total cell lysates were resolved by SDS-PAGE and immuno-blotted with the indicated antibodies. (*Lower panel)* Signals were quantified by densitometry and used to calculate the intensity of expression of HA-PDCD4 relative to that of GAPDH. Data are expressed as ratios of HA-PDCD4 to GAPDH for each experimental condition and represent means $\pm$ SE of the results of three experiments, including the one shown in the upper panel.

852 (G) Cell lysates from the experiment shown in F were bound to the cap analog m^7GTP
853 conjugated to beads, and after extensive washing bound proteins were resolved by SDS-
854 PAGE and immunoblotted with the indicated antibodies. (H) *(Upper panel)* Similar
855 experiment as in (A), except that, equal amounts of cell lysates were immunoprecipitated
856 with an anti-eIF4E antibody, or control mouse IgG1 (mIgG1). Immune complexes were
857 resolved by SDS-PAGE for analysis of eIF4G, eIF4A, and eIF4E as indicated. *(Lower*
858 *panel)* The signals were quantified by densitometry and used to calculate the intensity of
859 binding of eIF4G, and eIF4A to eIF4E. Data are expressed as ratios of eIF4G or eIF4A
860 to eIF4E for each experimental condition and represent means $\pm$ SE of the results of three
861 experiments, including the one shown in the upper panel. (I) Similar experiment as in
862 (C), except that, equal amounts of cell lysates were immunoprecipitated with an anti-
863 eIF4E antibody. Immune complexes were resolved by SDS-PAGE for analysis of eIF4G,
864 and eIF4A, and eIF4E as indicated. (J) Similar experiment as in (E), except that, equal
865 amounts of cell lysates were immunoprecipitated with an anti-eIF4E antibody, or control
866 mIgG1. Immune complexes were resolved by SDS-PAGE for analysis of eIF4G, and
867 eIF4A, 4E-BP1, and eIF4E as indicated. (K) Similar experiment as in (G), except that,
868 equal amounts of cell lysates were immunoprecipitated with an anti-eIF4E antibody, or
869 control mIgG1. Immune complexes were resolved by SDS-PAGE for analysis of eIF4G,
870 and eIF4A, and eIF4E as indicated.
871
872 **Figure 6: Effects of RSK1-mediated phosphorylation and degradation of PDCD4 on**
873 **IFNα dependent expression of ISG protein products.** (A) Serum starved KT1 cells
874 were either left untreated or were treated with IFNα for the indicated times, in the

875 presence or absence of MG132 or diluent for MG132 (DMSO). Cell lysates were
876 resolved by SDS-PAGE and immunoblotted with anti-PDCD4, $p21^{WAF1/CIP1}$, ISG15,
877 SLFN5, or anti-GAPDH antibodies. (B-D) Serum-starved KT1 cells were pretreated with
878 SL0101-1 for 3 hours and then treated with IFNα for the indicated times. The cells were
879 lysed and equal amounts of protein were resolved by SDS-PAGE and immunoblotted
880 with the indicated antibodies. (E-G) Serum-starved KT1 cells were treated with IFNα for
881 6 hours in presence or absence of SL0101-1. Expression of mRNA for *Isg15* (E),
882 *$p21^{WAF1/CIP1}$* (F), *and Slfn5* (G) genes was assessed by quantitative real-time RT-PCR.
883 The GAPDH transcript was used for normalization. Data are expressed as fold increase
884 over IFNα untreated samples and represent means ± S.E. of 3 experiments. (H) KT1 cells
885 were transfected with either control siRNA or siRNA specifically targeting RSK1, and
886 after serum starvation were either left untreated, or treated with IFNα, as indicated. The
887 cells were lysed and equal amounts of protein were resolved by SDS-PAGE and
888 immunoblotted with anti- RSK1, anti-PDCD4, anti-ISG15, or anti-GAPDH antibodies, as
889 indicated.
890
891 **Figure 7: Phosphorylation of PDCD4 on Ser67 is required for expression of ISG**
892 **protein products by IFNα.** (A): KT1 cells were transfected with either empty vector, or
893 HA-tagged wild-type PDCD4, or HA-tagged PDCD4 S67/71A mutant, serum starved and
894 treated or untreated with IFNα. Total cell lysates were resolved by SDS-PAGE and
895 immunoblotted with the indicated antibodies. (B-C) KT1 cells were transfected with
896 either control siRNA or siRNA specifically targeting PDCD4, and after serum starvation

were either left untreated or were treated with IFNα for the indicated times. Total cell lysates were resolved by SDS-PAGE and immunoblotted with the indicated antibodies.

Figure 8: Regulatory effects of PDCD4 ISG mRNA translation. (A**)** KT1 cells transduced with control shRNA or shRNA targeted human PDCD4 were either left untreated or treated with IFNα for 24 hours. Cell lysates were separated on 10-50% sucrose gradient, and OD at 254 nm was recorded. The OD at 254 nm is shown as a function of gradient depth for each treatment. (B-C) Polysomal fractions were collected as indicated in A and RNA was isolated. Quantitative real-time RT-PCR assays to determine *Isg15* (B), and *slfn5* (C) mRNA expression in polysomal fractions was conducted using *Gapdh* for normalization. Data are expressed as fold increase over IFNα-untreated samples and represent means ± SD of 3 independent experiments.

Figure 9: Regulatory effects of PDCD4 in the generation of the antileukemic effects of IFNα. (A) KT1 cells were transfected with either control siRNA or siRNA specifically targeting PDCD4, as indicated. The cells were subsequently plated in methylcellulose, in the absence or presence of IFNα, and leukemic CFU-L colony formation was assessed. Data are expressed as percentage of control colony formation of untreated samples for each condition and represent means ± S.E. of 4 experiments. (B) KT1 cells were transfected with the empty vector, PDCD4 wt, or PDCD4 S67/71A mutant, as indicated. The cells were subsequently plated in methylcellulose, in the absence or presence of IFNα, and leukemic CFU-L colony formation was assessed. Data

are expressed as percentage of control colony formation of untreated samples for each condition and represent means± S.E. of 6 experiments.

Figure 10: Regulatory effects of RSK1 and PDCD4 in the inhibitory properties of IFNα on normal bone marrow-derived myeloid precursors. (A) Normal CD34+ bone marrow-derived cells were transfected with either control siRNA or siRNA specifically targeting PDCD4, or siRNA specifically targeting RSK1 as indicated. The cells were subsequently plated in methylcellulose, in the absence or presence of IFNα. CFU-GM progenitor colonies were scored after 14 days in culture. Data are expressed as % control colony formation from untreated cells and represent means ± S.E. of 3 independent experiments. (B) Normal CD34+ bone marrow-derived cells were transfected with either the plasmid PCDNA3, or HA-tagged PDCD4 wt or, PDCD4 S67/71A mutant, and incubated in the absence or presence of IFN in clonogenic assays in methylcellulose, as indicated. CFU-GM progenitor colonies were scored after 14 days in culture. Data are expressed as % control colony formation from untreated cells and represent means ± S.E. of 4 independent experiments.

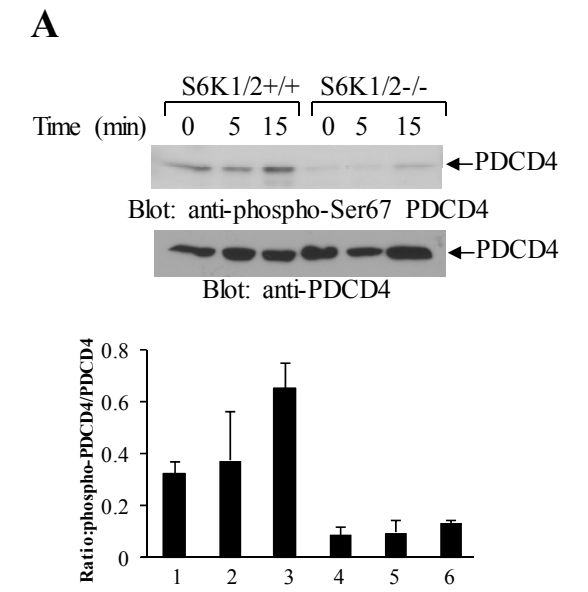

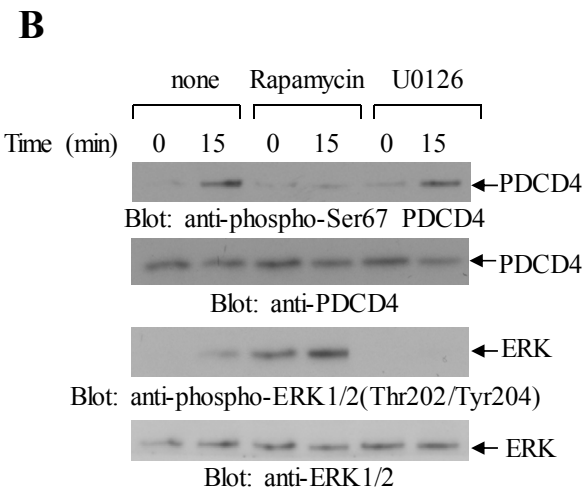

941

942 **Figure 1**

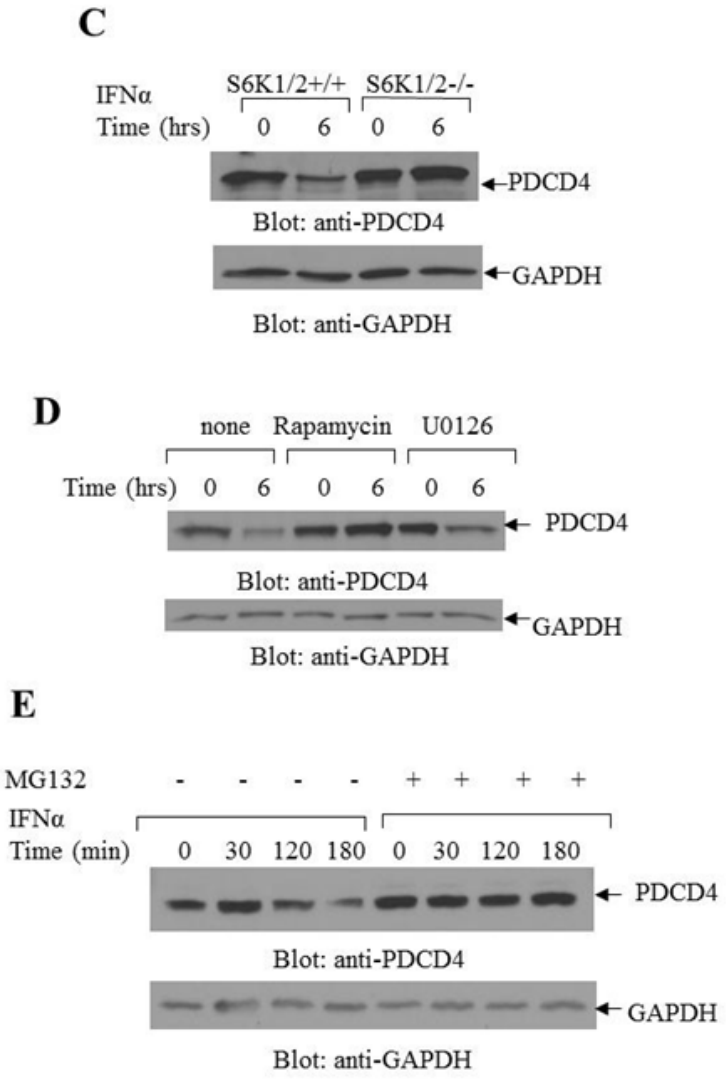

Figure 1

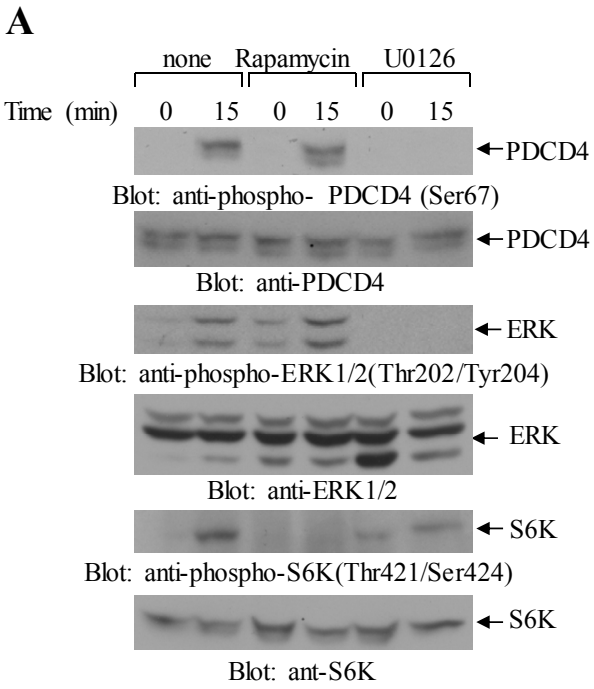

Figure 2

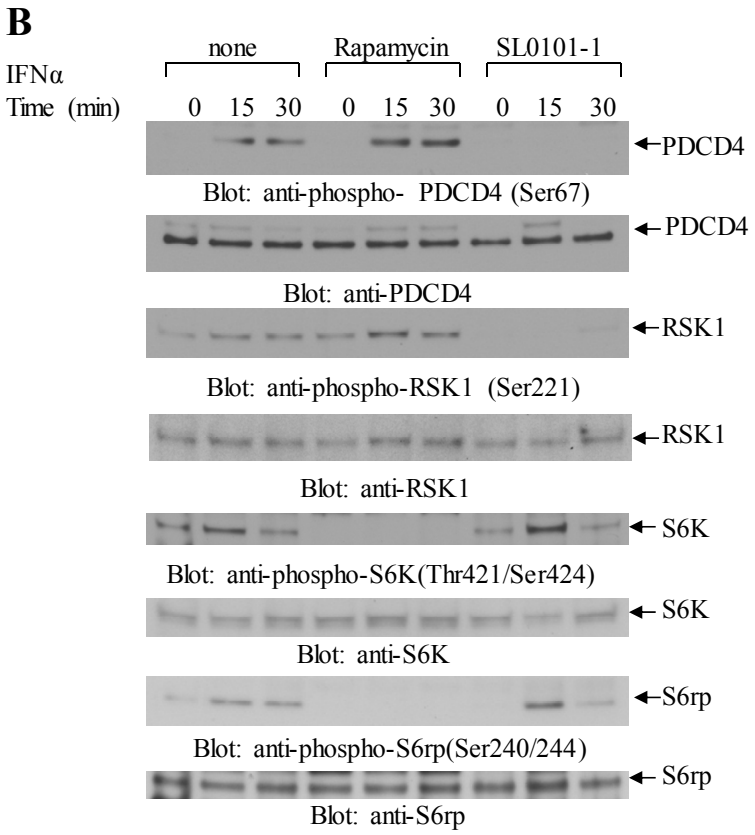

Figure 2

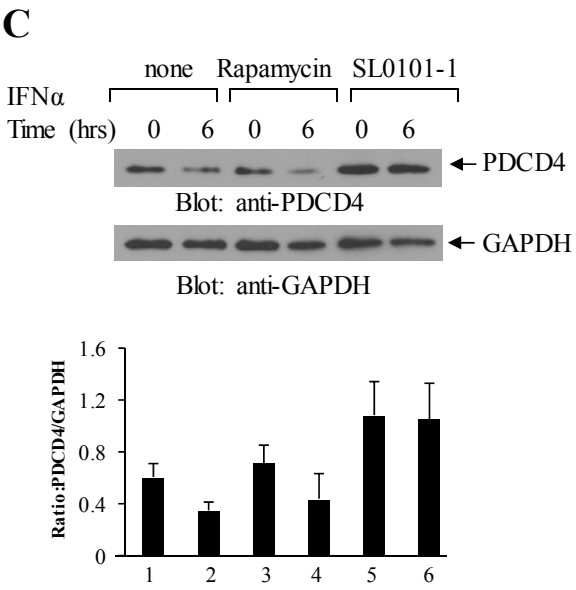

964

965

966

967 **Figure 2**

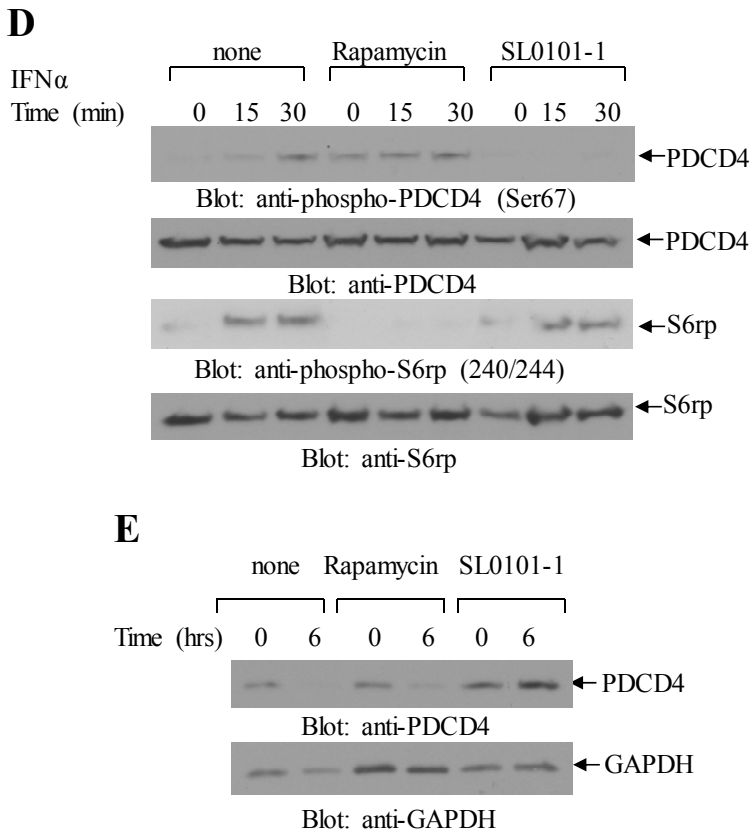

968

969

970

971 **Figure 2**

972

973

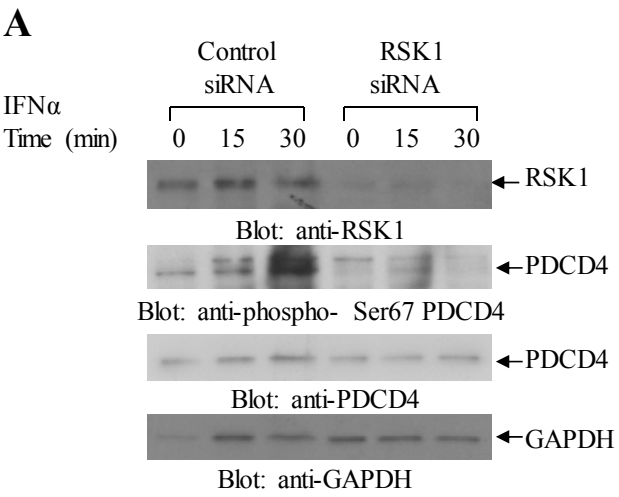

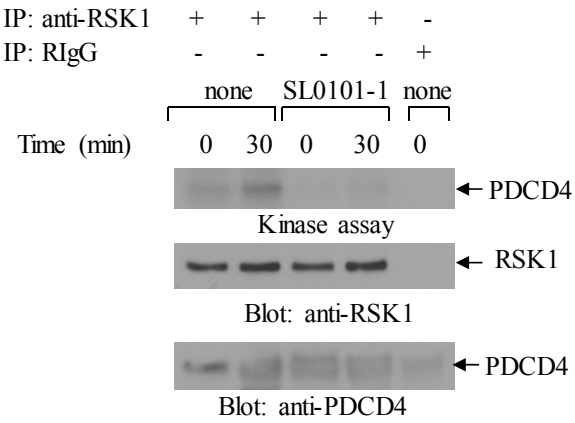

974

975 **Figure 3**

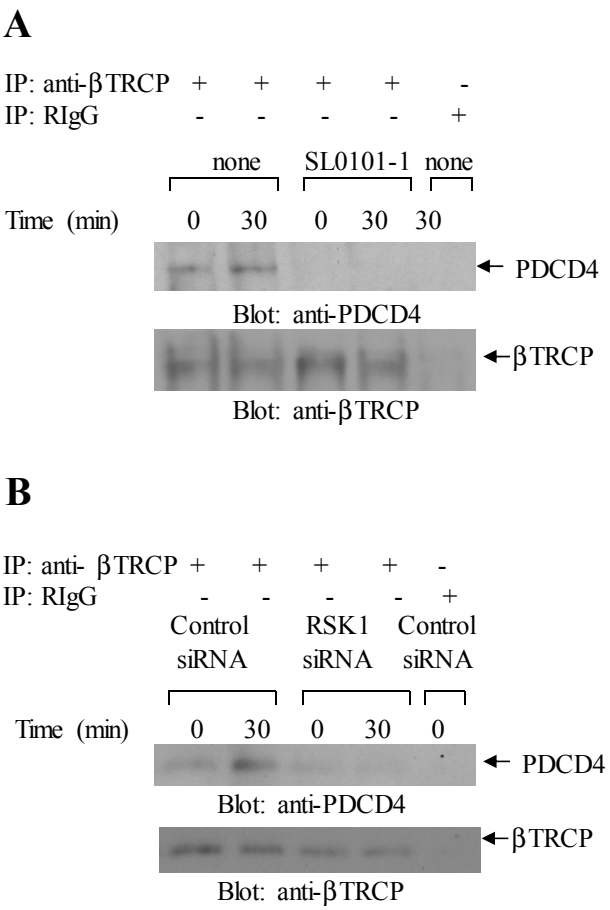

Figure 4

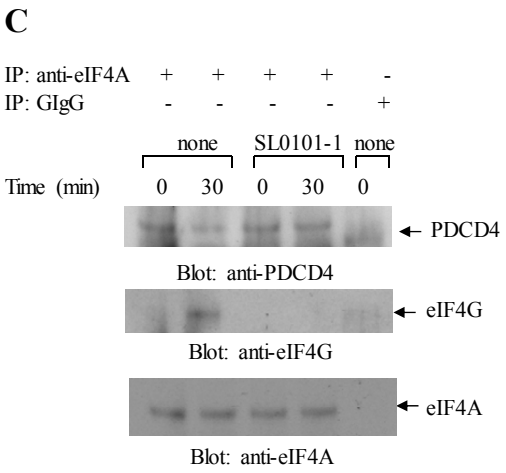

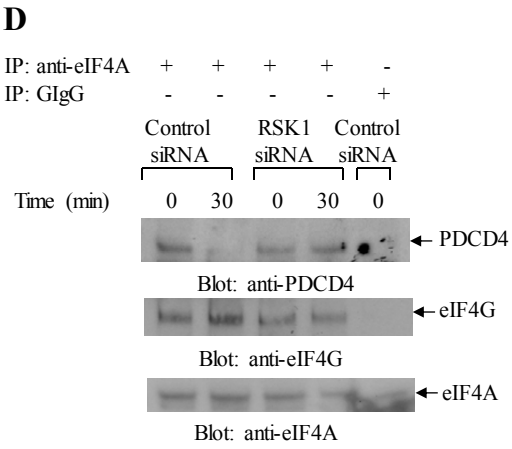

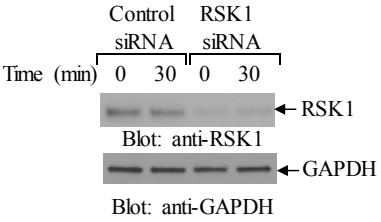

982

983 **Figure 4**

984

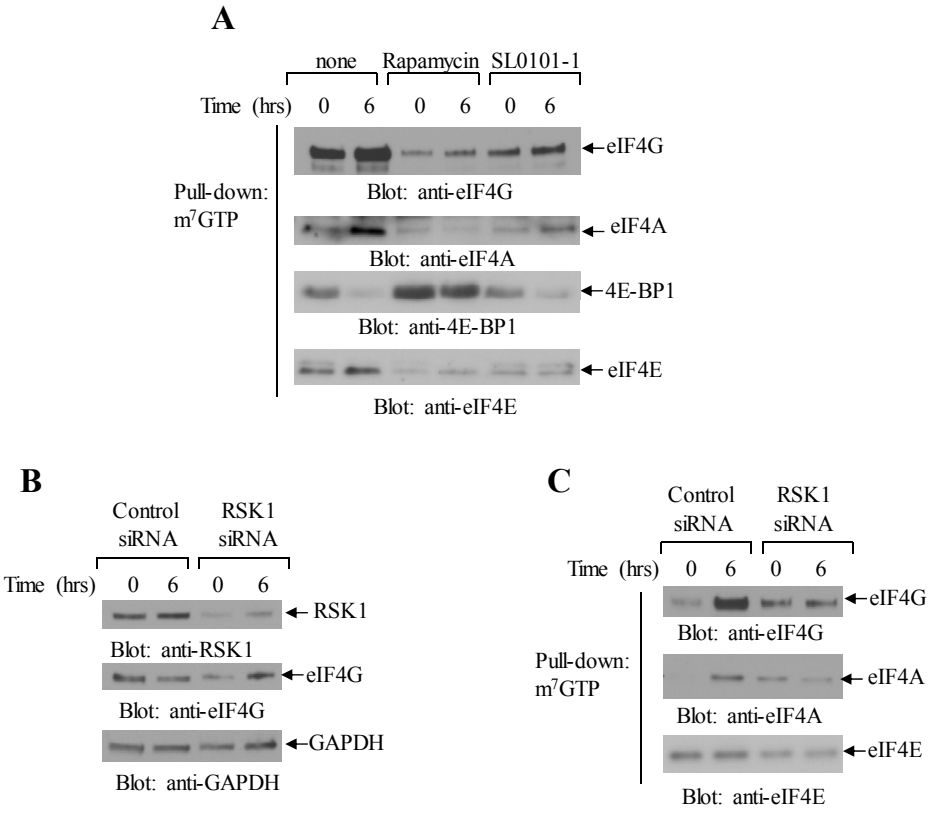

985

986

987

988 **Figure 5**

989

990

991

992

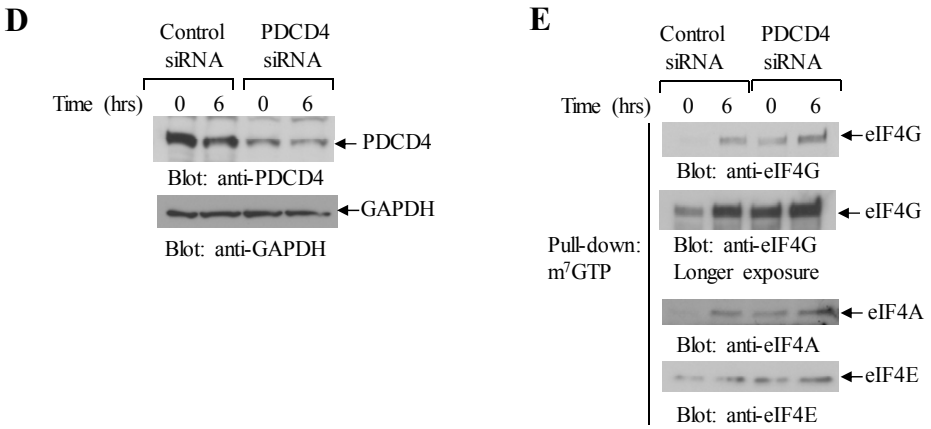

Figure 5

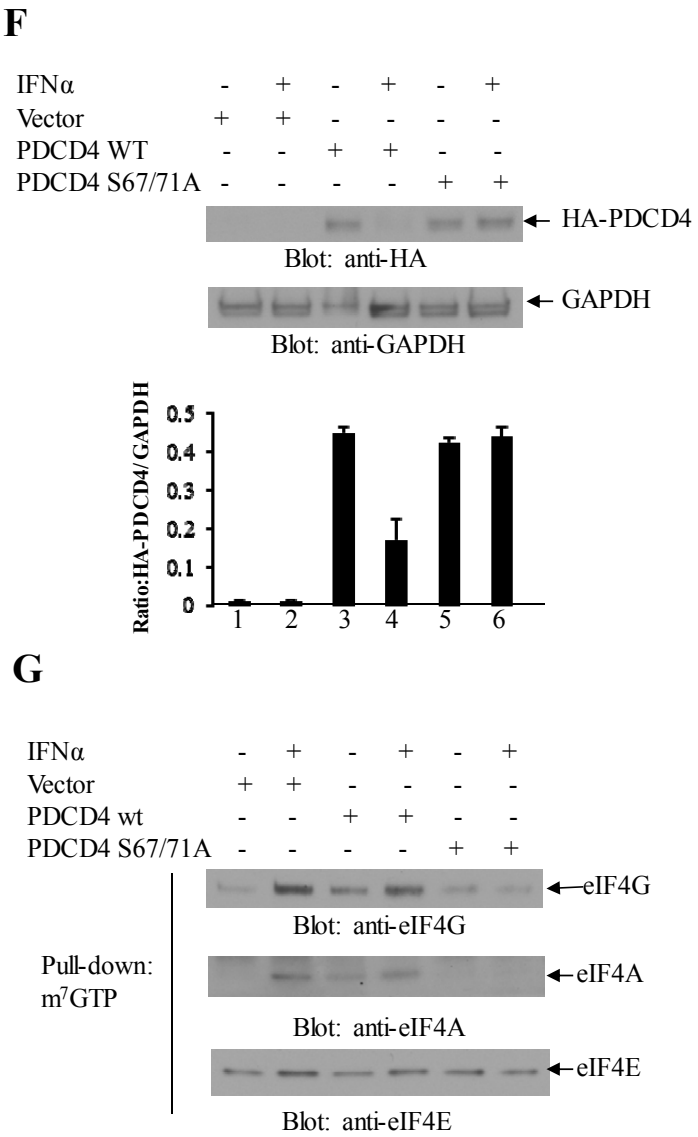

Figure 5

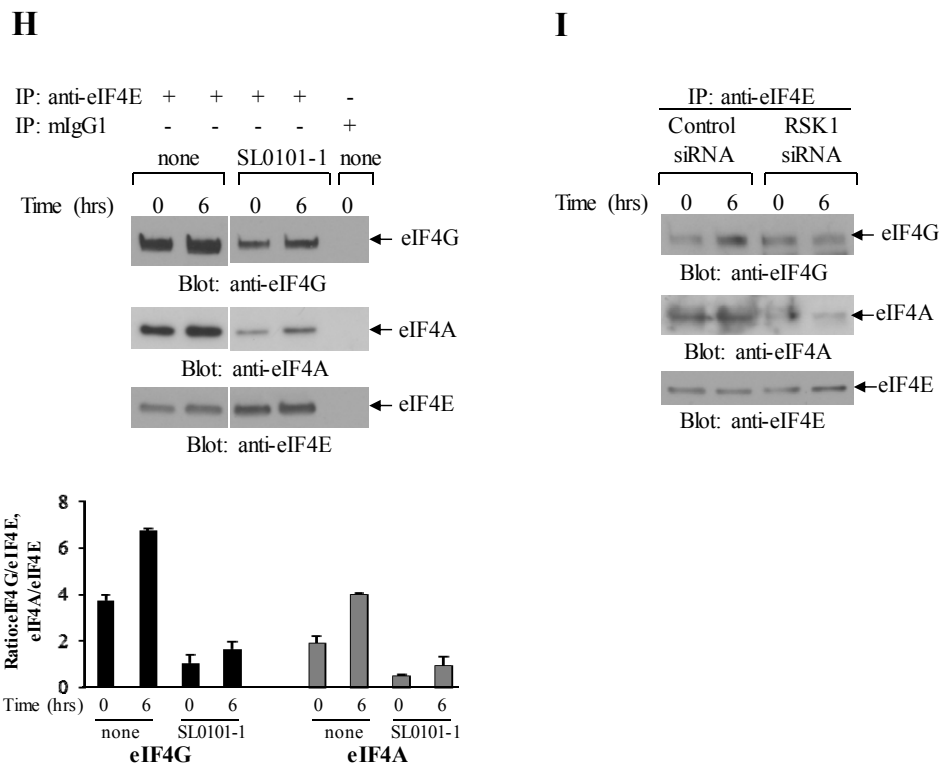

Figure 5

J

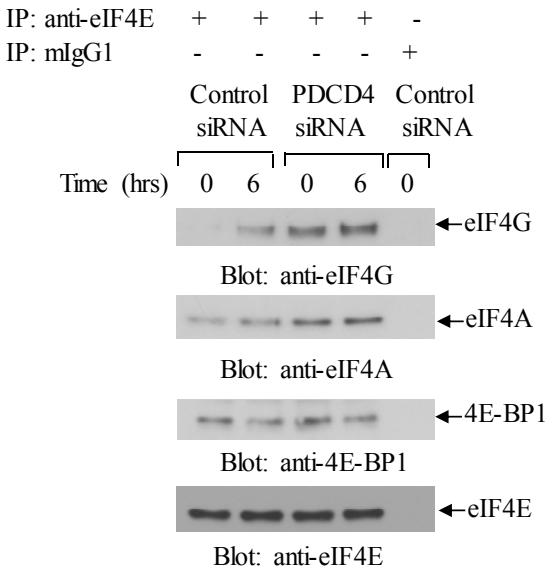

K

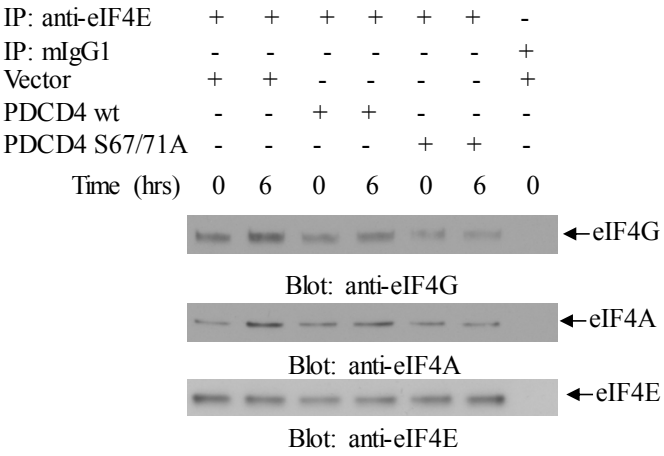

Figure 5

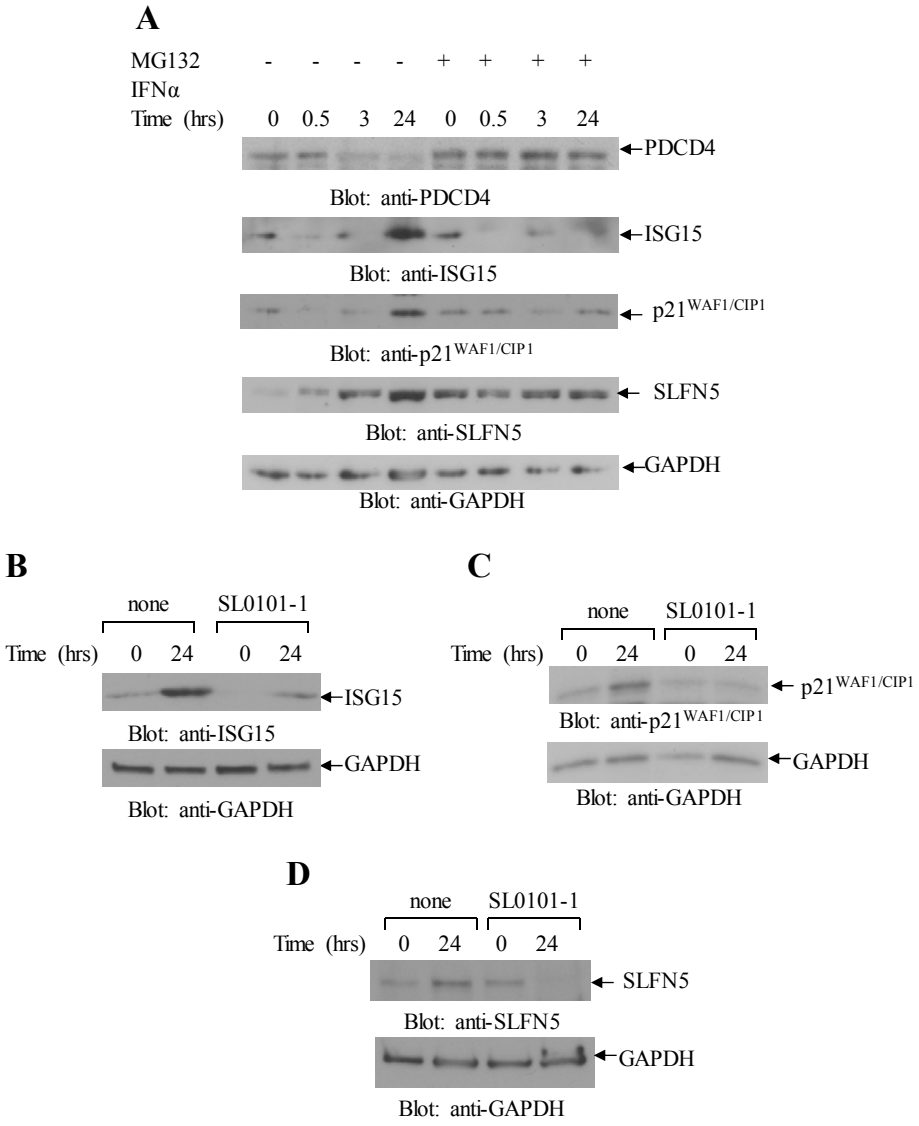

Figure 6

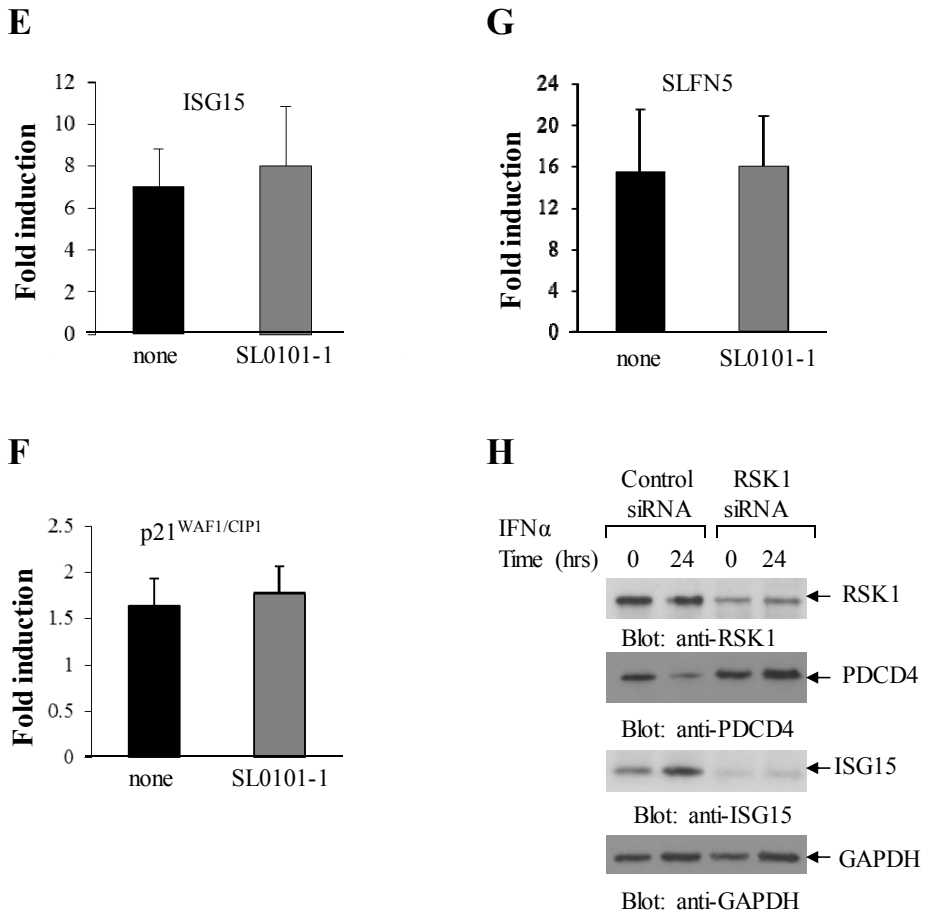

Figure 6

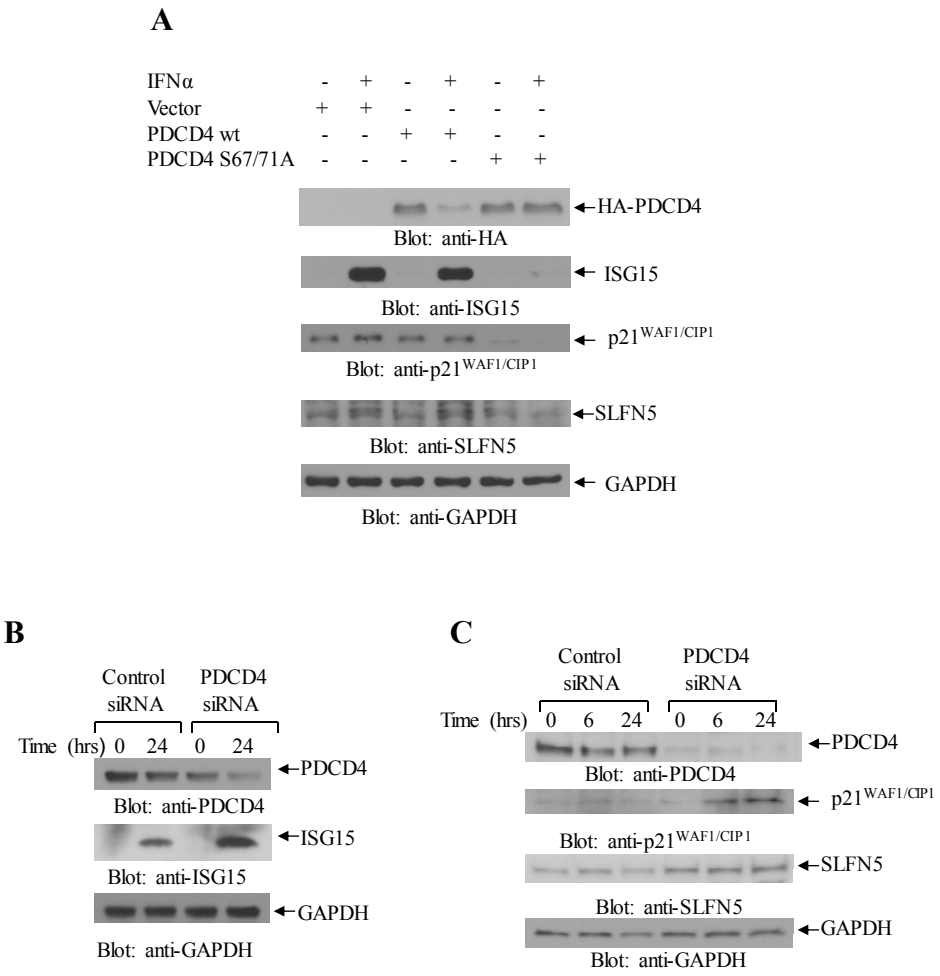

Figure 7

A

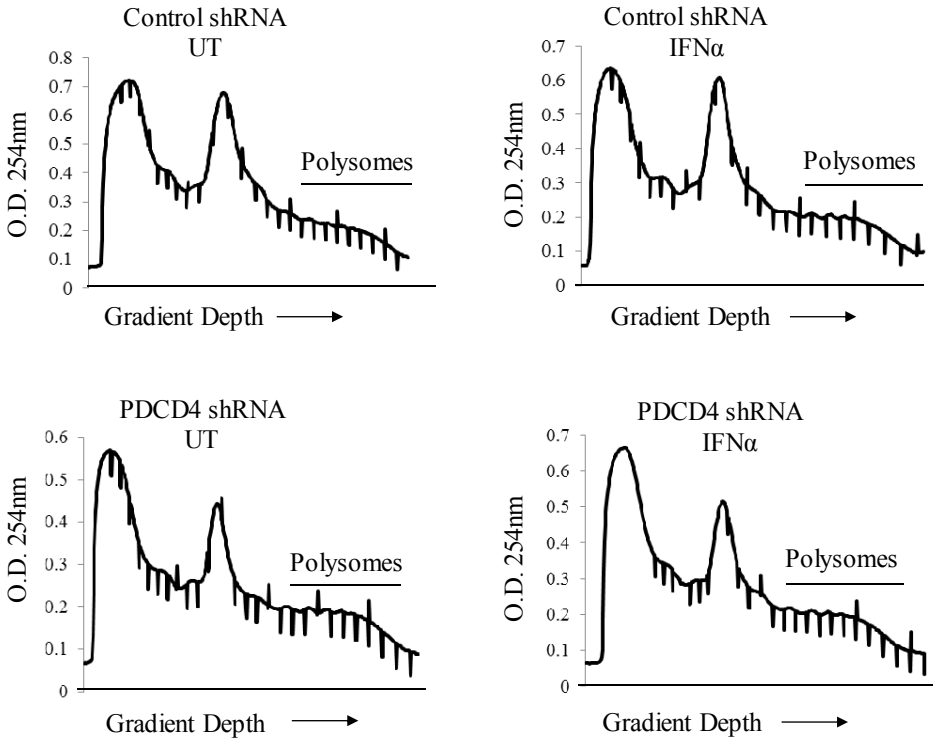

Figure 8

B

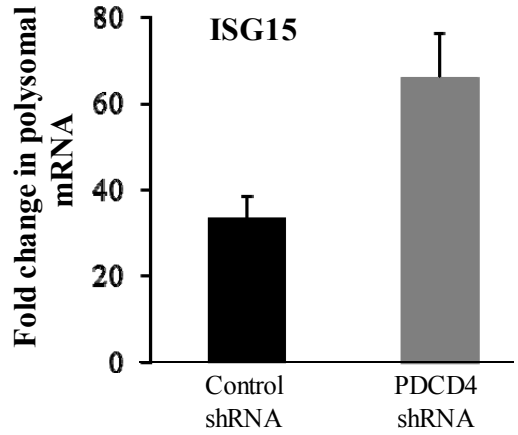

C

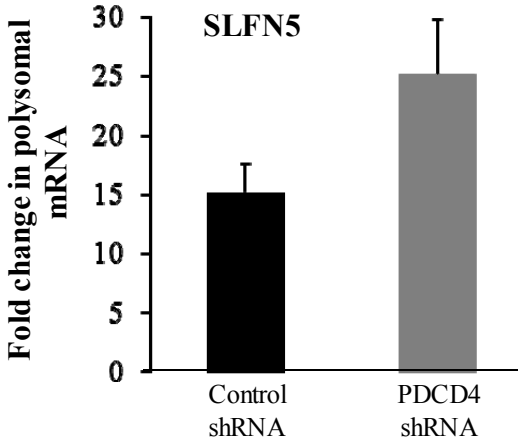

1040

1041

1042

1043 **Figure 8**

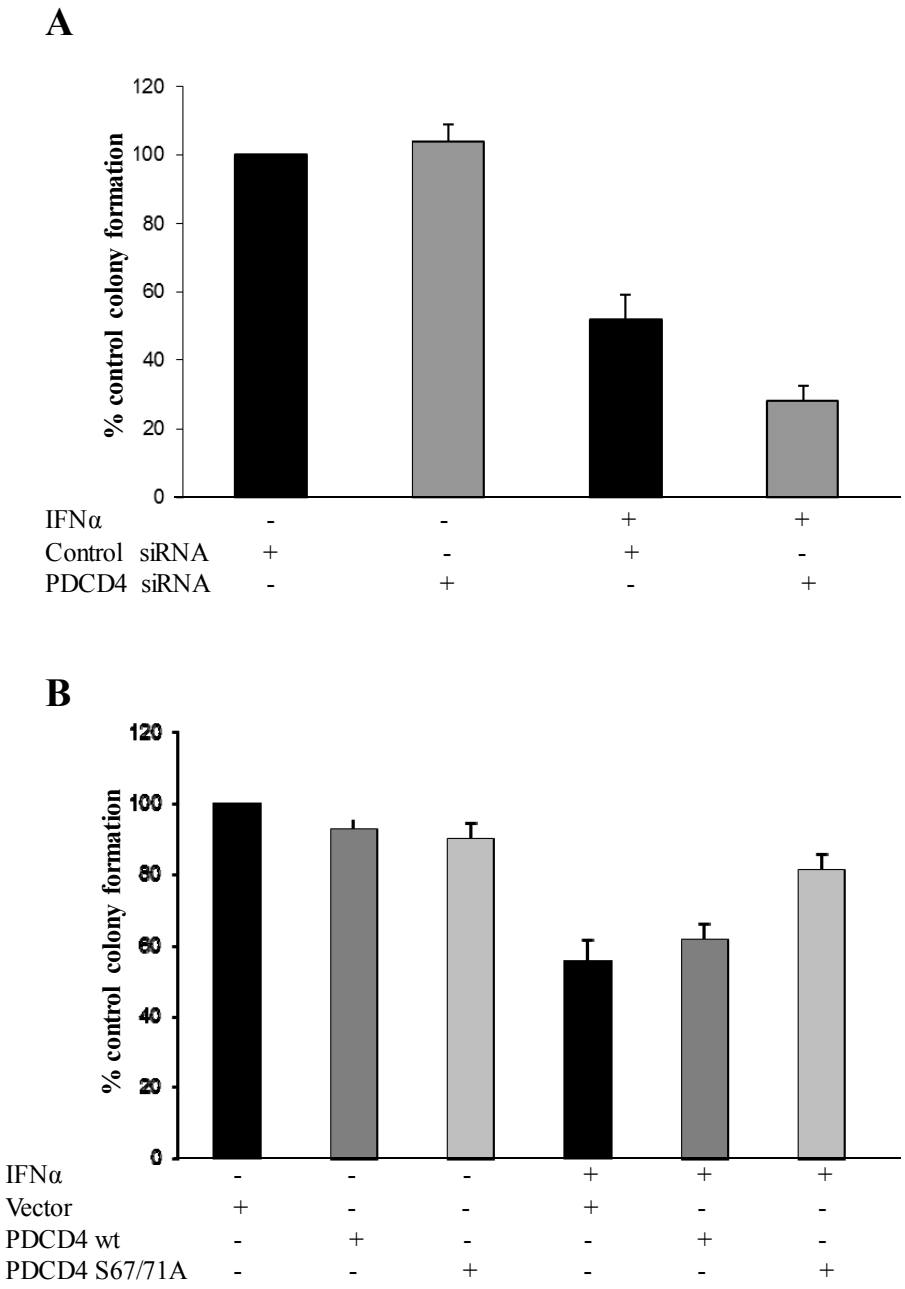

1044

1045 **Figure 9**

1046

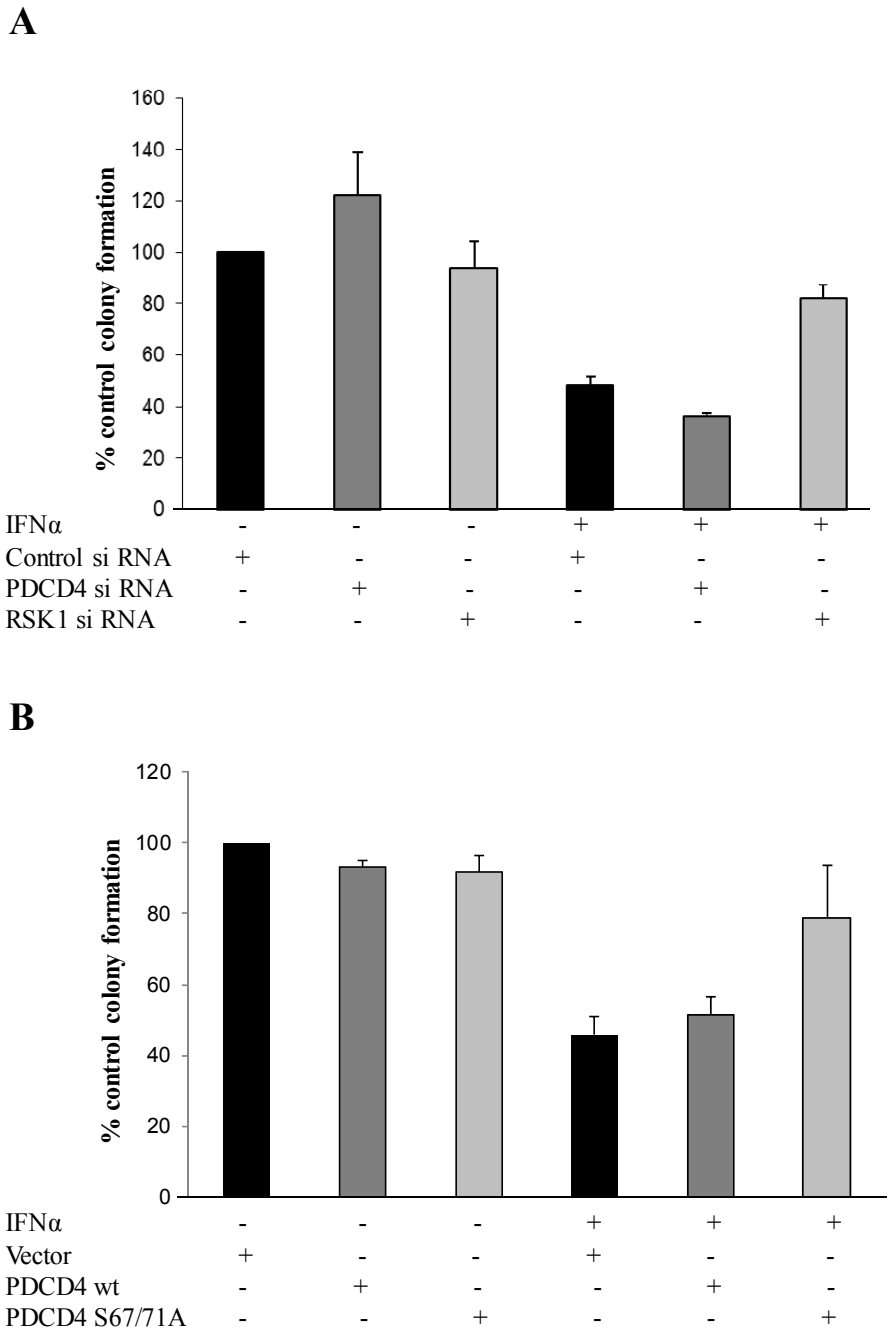

1047

1048 **Figure 10**